Title

Identification and Characterization of Genes Required for Compensatory Growth in Drosophila

Journal

Genetics, 189(4)

ISSN

0016-6731

Authors

Gerhold, Abigail R
Richter, Daniel J
Yu, Albert S
et al.

Publication Date

2011-12-01

DOI

10.1534/genetics.111.132993

Peer reviewed

Identification and Characterization of Genes Required for Compensatory Growth in *Drosophila*

Abigail R. Gerhold, Daniel J. Richter, Albert S. Yu, and Iswar K. Hariharan[1]
Department of Molecular and Cell Biology, University of California, Berkeley, California 94720-3200

ABSTRACT To maintain tissue homeostasis, some organs are able to replace dying cells with additional proliferation of surviving cells. Such proliferation can be localized (*e.g.*, a regeneration blastema) or diffuse (compensatory growth). The relationship between such growth and the growth that occurs during development has not been characterized in detail. *Drosophila melanogaster* larval imaginal discs can recover from extensive damage, producing normally sized adult organs. Here we describe a system using genetic mosaics to screen for recessive mutations that impair compensatory growth. By generating clones of cells that carry a temperature-sensitive cell-lethal mutation, we conditionally ablate patches of tissue in the imaginal disc and assess the ability of the surviving sister clones to replace the lost tissue. We have used this system together with a modified whole-genome resequencing (WGS) strategy to identify several mutations that selectively compromise compensatory growth. We find specific alleles of *bunched* (*bun*) and *Ribonucleoside diphosphate reductase large subunit* (*RnrL*) reduce compensatory growth in the imaginal disc. Other genes identified in the screen, including two alleles of *Topoisomerase 3-alpha* (*Top3α*), while also required for developmental growth, appear to have an enhanced requirement during compensatory growth. Compensatory growth occurs at a higher rate than normal growth and may therefore have features in common with some types of overgrowth. Indeed, the *RnrL* allele identified compromises both these types of altered growth and mammalian ribonucleotide reductase and topoisomerases are targets of anticancer drugs. Finally, the approach we describe is applicable to the study of compensatory growth in diverse tissues in *Drosophila*.

THE organs of multicellular eukaryotes typically reach a characteristic size and shape at the end of their developmental growth. Most organs derive from a small number of progenitor cells and the amount of growth undertaken by these cells is in accordance with an organ-intrinsic size-sensing mechanism (reviewed in Bryant and Simpson 1984; Conlon and Raff 1999). However, in response to tissue damage, surviving cells are often required to undergo extra divisions to replace tissue that has been lost. When a large and contiguous portion of an organ has been removed, this extra growth is referred to as regeneration, which typically involves the formation of a blastema, a zone of progenitor and/or stem cells that proliferate extensively to replace the lost tissue mass (Stoick-Cooper *et al.* 2007; Brockes and Kumar 2008). In contrast, compensatory proliferation (Fan and Bergmann 2008; Bergmann and Steller 2010) has been used to describe a phenomenon where the death of individual cells scattered through a tissue elicits additional proliferation in the surviving cells without the formation of a distinct blastema.

The characteristics of regenerative and compensatory growth are likely to differ, at some level, from the growth that occurs during normal development. During development, growth and patterning often proceed concurrently. In contrast, regeneration and compensatory proliferation often occur in the context of a fully or partially patterned structure and are stimulated by local injury. In both cases, cells that have activated the apoptotic pathway appear necessary for the extra proliferation (Huh *et al.* 2004; Perez-Garijo *et al.* 2004; Ryoo *et al.* 2004; Tseng *et al.* 2007; Chera *et al.* 2009; Pellettieri *et al.* 2010). Thus, an important and unresolved question is whether there are genetic pathways that specifically regulate regeneration and compensatory proliferation. Alternatively, pathways that are required for growth under normal conditions may function in different ways or at different levels during regeneration or compensatory proliferation.

doi: 10.1534/genetics.111.132993
Manuscript received July 21, 2011; accepted for publication September 12, 2011
Available freely online through the author-supported open access option.
Supporting information is available online at http://www.genetics.org/content/suppl/2011/09/16/genetics.111.132993.DC1.
[1]Corresponding author: Department of Molecular and Cell Biology, University of California, Berkeley, 361 LSA, Berkeley, CA 94720-3200. E-mail: ikh@berkeley.edu

Drosophila imaginal discs, the precursors of adult structures such as the eye and the wing, offer an excellent opportunity to study regenerative or compensatory growth. They develop from primordia composed of 15–40 cells and typically experience a 1000-fold increase in cell number over larval development (Bryant and Simpson 1984). Larval imaginal discs show remarkable regenerative capacity. Damage from irradiation, surgical injury, or genetic ablation, elicits additional cell proliferation producing normally sized and patterned adult organs (Hadorn and Buck 1962; Haynie and Bryant 1977; Milan *et al.* 1997; Smith-Bolton *et al.* 2009).

Surgical injury to imaginal discs results in the formation of a blastema (Abbott *et al.* 1981; Kiehle and Schubiger 1985; O'Brochta and Bryant 1987) as does the ablation of a large portion of the wing imaginal disc *in situ* using a genetic method (Smith-Bolton *et al.* 2009). Less localized damage to imaginal discs, as occurs upon treatment with X-ray irradiation, stimulates compensatory proliferation in the surviving cells (Haynie and Bryant 1977; Jaklevic and Su 2004; Halme *et al.* 2010). To understand whether dying cells directly stimulate the proliferation of surrounding cells, several investigators have blocked the death of apoptotic cells by expressing the baculovirus p35 protein, an inhibitor of effector caspases. These "undead" cells appear to stimulate cell proliferation nonautonomously by expressing secreted proteins such as Wingless (Wg) and Decapentaplegic (Dpp) (Huh *et al.* 2004; Perez-Garijo *et al.* 2004; Ryoo *et al.* 2004). The presence of undead cells, however, may not fully reflect a normal physiological response to tissue damage. Indeed, a recent study has suggested that neither *dpp* nor *wg* are required for irradiation-induced compensatory growth when dying cells complete apoptosis and are cleared normally from the epithelium (Perez-Garijo *et al.* 2009). Thus the mechanisms that stimulate compensatory proliferation are still poorly understood.

It is therefore necessary to examine compensatory proliferation in a context that does not depend upon the generation of undead cells. Moreover, current systems to study regeneration in imaginal discs, both surgical and genetic, have not yet been adapted to allow for the discovery of loss-of-function mutations that alter regeneration. Finally, mosaic screens for recessive mutations have proven a powerful tool in the identification of genes that function during normal imaginal disc growth (St Johnston 2002). Yet these types of screens have not been applied to study regenerative or compensatory growth.

Here we describe a system that uses genetic mosaics to conditionally ablate patches of cells within the developing imaginal disc and thereby induce regenerative or compensatory growth. We have used this method to characterize the properties of this additional growth and to conduct a screen for recessive mutations that impair it. Using an approach based on whole-genome resequencing (WGS) we have identified several of the affected genes from our screen. Our results show that ablating patches of cells induces diffuse compensatory growth rather than a localized regeneration blastema. This compensatory growth is in part an acceleration of developmental growth and thus sensitizes cells to reduced levels of factors required for more rapid growth. Interestingly, two of the genes that we have identified are also common chemotherapeutic targets. Additional characterization of a set of our mutants suggests that these mutations may interfere with compensatory growth in different ways and that at least one also curtails tissue overgrowth.

Materials and Methods

Drosophila stocks and transgenes

The *sec5^{ts}* wing disc ablation system was generated by recombination of the following: *sec5^{ts1}* (Murthy *et al.* 2010), *FRT40A*, *en-GAL4* (BL30564), and *UAS-FLP* (BL4539). The experimental fly stocks used were *w*; *sec5^{ts1}*, *FRT40A*, *en-GAL4*, *UAS-FLP/SM6-TM6B*, *w*; *FRT40A*, *en-GAL4*, *UAS-FLP*, and *w*; *P{mw+, ubi-GFP.nls}*, *FRT40A*. The eye disc ablation system used *y*, *w*, *ey-FLP*; *sec5^{ts1}*, *FRT40A/SM6-TM6B*. The EMS screen was carried out using an isogenized stock of *w*; *P{mw+, ubi-GFP.nls}*, *FRT40A*. For clonal growth assays in the eye in the absence of ablation and for testing mutations for defects in X-ray irradiation-induced compensatory growth the stock *y*, *w*, *ey-FLP*; *FRT40A* was used. The mosaic analysis with a repressible cell marker (MARCM) experiment used the following stocks: *w*, *UAS-mCD8::GFP*, *hs-FLP122*; *tub-GAL80*, *FRT40A*; *tub-GAL4/TM6B* (Wu and Luo 2006) ("MARCM tester"), *w*; *P{mw+, ubi-GFP.nls}*, *FRT40A*; *UAS-yorkie^{S168A}*, *w*; *RnrL^{A4B5}*, *P{mw+, ubi-GFP.nls}*, *FRT40A/CyO*; *UAS-yorkie^{S168A}*, *w*; *P{mw+, ubi-GFP.nls}*, *FRT40A*, and *w*; *RnrL^{A4B5}*, *P{mw+, ubi-GFP.nls}*, *FRT40A/CyO*; *TM6B/TM2*. *UAS-yorkie^{S168A}* expresses a mutant hyperactivated form of the Yorkie protein (Oh and Irvine 2008).

sec5^{ts} wing disc ablation

Experimental animals were generated by the crosses *w; sec5^{ts1}, FRT40A, en-GAL4, UAS-FLP/SM6-TM6B* X *w; P{mw^{+}, ubi-GFP.nls}, FRT40A* for "ablated" discs/wings and *w; FRT40A en-GAL4, UAS-FLP* X *w; P{mw^{+}, ubi-GFP.nls}, FRT40A* for "control" discs/wings. Unless otherwise noted, all experiments were carried out according to the following protocol. Eggs were collected on agar grape juice plates at room temperature for 4–6 hr. Plates were moved to 18° for 48 hr after which L1 larvae were transferred, 55 per vial, to standard fly food supplemented with fresh yeast paste. Vials were shifted to 30° 7.5 days AEL for 48 hr. Discs were dissected at certain time points during the ablation period or animals were returned to 18° and adult wings were collected after eclosion. Control and ablated animals were subjected to the same treatment.

Immunohistochemistry and image processing

Discs were dissected in PBS and fixed for 20 min at room temperature in 4% paraformaldehyde. Antibody stains were

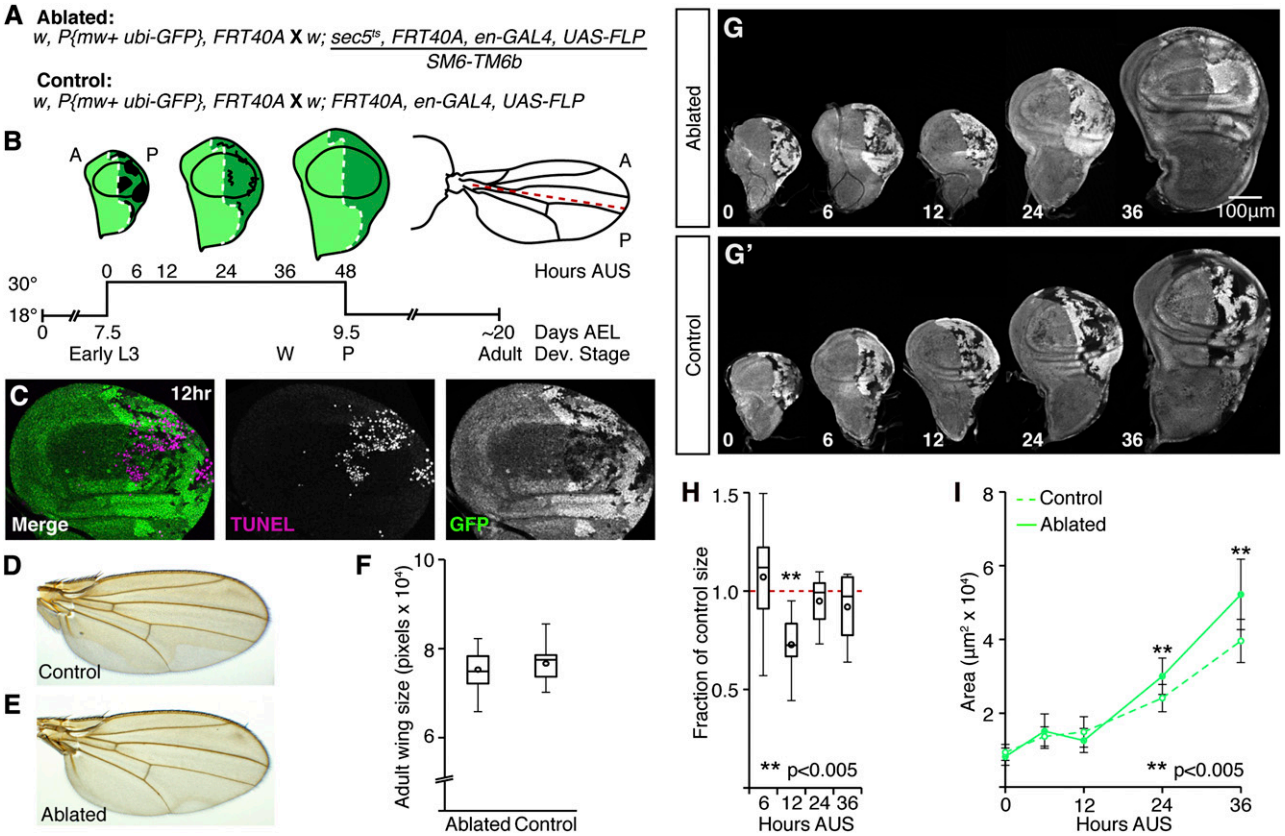

Figure 1 Mosaic system to study compensatory growth in *Drosophila* imaginal discs. We will hereafter refer to mosaic discs with *sec5*^{ts1} mutant clones as ablated discs and mosaic discs with nonablating control clones as control discs. (A) Genetic crosses used to generate the ablated and control animals used for study. (B) Schematic showing the *sec5*^{ts} system. (C) High levels of apoptosis were observed in ablating discs. Discs are shown at 12 hr after upshift (AUS). TUNEL (magenta) was used to label apoptotic cells. *sec5*^{ts}/*sec5*^{ts} cells were marked by the absence of GFP (green). Posterior is to the right. (D–F) After eclosion, ablated wings were approximately the same size as nonablated controls. Adult wings from a control adult (D) and an ablated adult (E). (F) Quantification of adult wing size. All graphical data are presented in a "box and whiskers" format (see *Materials and Methods*) unless otherwise stated. (G and H) Ablated discs were smaller than control discs 12 hr AUS, but regained normal size by 36 hr AUS. (G and G′) Discs dissected from control (G) or ablated (G′) animals. Posterior is to the right. (H) Quantification of ablated posterior compartment size expressed as a fraction of the average control size (red dashed line at 1). (I) Between 12 and 36 hr AUS, the GFP$^+$ tissue in *sec5*^{ts} discs increased in size more than the corresponding tissue in control discs. The area ($\mu m^2 \times 10^4$) of GFP$^+$ tissue in the posterior compartment is shown. Data points represent the average area. Error bars denote 1 SD. The predicted rate of growth between 12 and 36 hr AUS is 1.65×10^3 μm^2/hr for ablated discs and 1.03×10^3 μm^2/hr for control discs.

performed according to standard methods. We used mouse anti-GFP (1:500; Roche) and rabbit anti-phosphohistone H3 (PHH3) (1:200; Upstate). All secondary antibodies were Alexa Fluor antibodies (1:500; Invitrogen). Cell death was assessed using a TUNEL kit (Roche) and the labeling reaction was conducted for 1 hr at 37°. Nuclei were visualized using DAPI. Images were captured on a Leica TCS SL or a Zeiss LSM 700 confocal and were processed using ImageJ and Adobe Photoshop.

Image analysis and quantification

For adult wing size (Figure 1E), wings from 20–25 ablated and control males were removed and mounted in Gary's Magic Mountant. Wings were imaged on a Leica Z16 APO microscope. Quantification was done in Adobe Photoshop. The entire wing area was selected using the "quick selection tool" and the number of pixels was assessed using the "record measurements" function. For posterior compartment size and area of GFP$^+$ and GFP$^-$ tissue (Figures 1, G and H, and 7E), discs were imaged on a Zeiss LSM 700 confocal microscope. Quantification was done in Volocity. The posterior compartment was selected manually on the basis of GFP expression and the area of the entire compartment or the GFP$^+$ area was measured using the Volocity object recognition software. The GFP$^-$ area was calculated on the basis of these two values. We estimated the rate of growth of the GFP$^+$ tissue from the slopes ($\mu m^2 \times 10^3$/hr) of the ablated and control lines between the 12- and 36-hr AUS data points. At least nine ablated and control discs were analyzed for each time point. A second independent experiment yielded similar results (data not shown). For the density of mitotic cells (Figure 2E), discs were imaged on either a Leica TCS SL or a Zeiss LSM 700. A z-series of confocal slices was obtained through the entire disc proper epithelium. Phosphohistone H3$^+$ cells were counted either from a z-max projection of all focal planes, manually using the Image

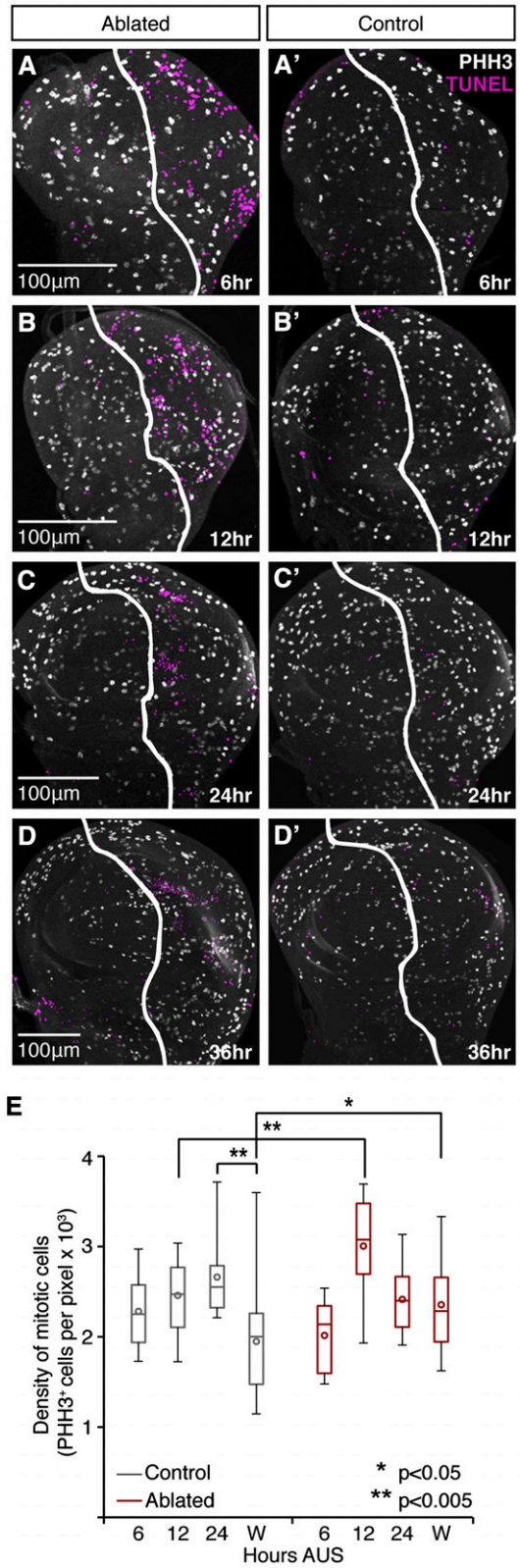

Figure 2 *sec5*^{ts} ablation produces nonlocalized compensatory proliferation. (A–D) Discs were dissected at different time points after upshift and stained with anti-phosphohistone H3 (PHH3, white) to mark mitotic cells and TUNEL (magenta) to mark apoptotic cells. Ablated discs are at left (A–D) and control discs at right (A′–D′). Images are *z*-max projections of confocal slices through the entire disc epithelium. White lines mark the approximate A–P boundary as assessed by GFP levels. (A and A′) Apoptotic cells were observed as early as 6 hr AUS. (B and B′) High levels of apoptosis were seen at 12 hr AUS; however, no consistent colocalization between mitotic and apoptotic cells was observed. At least 20 discs from two independent experiments were examined. (C and C′) Levels of apoptosis declined by 24 hr AUS. (D and D′) By 36 hr AUS, most TUNEL staining was found in residual cellular debris (small puncta present only in very basal confocal sections). More mitotic cells are visible in ablated discs than in controls. (E) Quantification of the density of mitotic cells, as marked by PHH3. Ablated discs are shown in red. Control discs are shown in gray.

"cell counter" plug-in, or from a 3D reconstructed image in Volocity using the object recognition software. For each disc the entire posterior compartment was analyzed. The density of mitotic cells was then calculated by dividing the total number of mitotic cells by the area of the posterior compartment. Data were combined from two independent experiments each with at least nine ablated and control discs for each time point. Unless otherwise noted, all data were reported as box and whiskers plots in which boxes mark 25th and 75th quartiles, whiskers show high and low values, and open circles show the mean. Statistical analysis was performed using a Student's two-tailed *t*-test.

EMS mutagenesis and screen of chromosome 2L

Three- to four-day-old *w*; *P{mw+, ubi-GFP.nls}*, *FRT40A* males were starved for 8 hr and then fed a 25-mM ethyl methanesulfonate solution in 1% sucrose for ~16 hr. Mutagenized males were crossed in bulk to *y*, *w*, *ey-FLP*; *sec5*^{ts1}, *FRT40A/SM6-TM6B* virgin females. Eggs were collected on agar grape juice plates for two 6- to 8-hr collections a day at room temperature and one overnight ~12-hr collection at 18°. Mutagenized males were removed from the cross after 5 days. Plates were placed at 18° and after 48 hr, freshly hatched L1 larvae were transferred, 55 per vial, to fly food supplemented with fresh yeast paste. Seven days after egg laying (AEL), vials were shifted to 30° for 40–44 hr, after which they were returned to 18°. Single F_1 males of the genotype *y*, *w*, *ey-FLP*; * *P{mw+, ubi-GFP.nls}*, *FRT40A/sec5*^{ts1}, *FRT40A* showing a reduced eye phenotype were each crossed back to 10–15 *y*, *w*, *ey-FLP*; *sec5*^{ts1}, *FRT40A/SM6-TM6B* virgin females. Eggs were collected directly in vials for 8- to 10-hr periods at room temperature. Vials were then transferred to 18°. One set of F_2 progeny was maintained at 18° until adult eclosion and was screened for a reduction in the amount of red (mutant) tissue present in the adult eye. A second set was shifted to 30° for 40–44 hr ~7 days AEL and rescreened for the reduced eye phenotype. If the desired phenotype was observed, F_2 males were crossed either to *w*; *Sp/CyO* or *w*; *Sp*; *Dr/SM6-TM6B* virgin females to establish stable stocks.

Clonal growth analysis in the adult eye

Experimental animals were generated by crossing virgin female *y*, *w*, *ey-FLP*; *FRT40A* to individual mutants (* *P{mw+, ubi-GFP.nls}*, *FRT40A*) or the nonmutagenized isogenic parent

(*P{mw+, ubi-GFP.nls}, FRT40A*). Eggs were collected directly in vials for ~10–12 hr at 25°. One set of vials was maintained at 25°. Another set of vials was shifted to 30° 3 days AEL until adult eclosion. A third set of vials was treated with X-ray irradiation 3 days AEL by placing the vials in a cabinet X-ray (Faxitron TRX5200) and irradiating for 20 min at 125 V and 3 mA for an approximate dose of 33 Gy. Animals from 2–3 egg collections from different days were analyzed for each treatment.

Illumina WGS

Genomic DNA was isolated from 10 gut-evacuated wandering third instar larvae per genotype, as described by Blumenstiel *et al.* 2009. Illumina libraries (ab, bc, and ac) were prepared according to the Illumina paired-end sample preparation guide with the following modifications. All reagents were purchased from NEB, except dATP, which was from Fisher. PCR primers were from IDT and adapters from Illumina. A total of 10–20 μg of DNA was sheared by sonication in a Bioruptor (Diagenode) at 4°, in 200 μl of TE for 30 min with 30-sec on/off pulses. For the ab and bc libraries, sonicated DNA was run out on a 1.5% agarose gel and fragments 200–300 bp in length were selected. For the ac library, no size selection step was added. For all libraries, a final size-selection step was added after the PCR to remove presumed primer dimer products. Libraries were sequenced on an Illumina GAII sequencer for 36-bp reads. ab and bc were sequenced on one lane using single-end reads and on one lane using paired-end reads. ac was sequenced on two lanes using paired-end reads.

WGS data analysis and SNP discovery

All Illumina reads were mapped to the 5.25 release of the *Drosophila melanogaster* genome with MAQ version 0.7.1 (Li *et al.* 2008; maq.sourceforge.net) using default parameter values. The .pileup and .snp MAQ output files were analyzed further using a series of custom Perl scripts. The .pileup file was used to determine coverage along 2L. We combined information from the .pileup and .snp files into one comprehensive mutation list. We disallowed any mutation with a sequencing quality score <20 and any that occurred within the first 5 bp of a read. To find mutations unique to each genotype, we generated data sets by intersecting mutations from two libraries and excluding mutations from the third. We did not consider mutations with an allele frequency <0.1, a mutant allele count <2, and those at positions where the average number of mapping hits for reads mapped to the position (average hits) was >1. For our analysis of all combined reads (ABC), we generated a mutation list by setting the following cutoffs: an allele frequency between 0.2 and 0.8, a minimum read depth of 4, average hits ≤ 1, and a MAQ consensus quality score of 40. Mutation lists resulting from all analyses were refined to include only nonsynonymous protein coding mutations. We then used SIFT (Kumar *et al.* 2009; sift.jcvi.org) to predict whether a nonsynonymous mutation was likely to be deleterious or tolerated. Candidate mutations were confirmed by Sanger sequencing following PCR amplification of the desired region.

MARCM clone generation

Eggs were collected directly in vials for 4–6 hr at 25°. Vials were heat shocked at 37° for 15 min ~48 hr AEL. Wandering larvae were selected for dissection 120 hr AEL. After dissected discs were mounted on slides, samples were given an arbitrary label and all subsequent imaging and data analysis was carried out blind. A series of 3–5 discs, with at least five clones each, were imaged for each sample and qualitative assessment of clone size and features were made prior to genotype assignment.

Results

A mosaic system to study compensatory growth in Drosophila imaginal discs

To develop a system that would allow us to study regenerative or compensatory growth in imaginal discs, we took advantage of FLP/FRT-catalyzed mitotic recombination and a temperature-sensitive recessive cell-lethal mutation. This allowed us to generate patches of tissue that could be ablated upon shifting to the restrictive temperature (30°). Thus, to achieve a disc of the appropriate final size, the surviving cells must undergo additional proliferation. We used *engrailed-GAL4* (*en-GAL4*) to drive expression of a *UAS-FLP* transgene and a temperature-sensitive recessive cell-lethal mutation in the *sec5* gene ($sec5^{ts1}$, hereafter $sec5^{ts}$) on an FRT chromosome (Langevin *et al.* 2005; Murthy *et al.* 2010). We generated clones by crossing these animals to a line with a wild-type FRT chromosome that also carried a copy of GFP (Figure 1A).

In the wing disc, *en* is expressed early and continuously in the posterior compartment, with an additional stripe of expression just anterior to the anterior–posterior (A–P) compartment boundary late in larval development (Blair 1992). This allowed us to generate discs in which the posterior compartment was composed almost entirely of two populations of cells: mutant $sec5^{ts}$ clones, marked by the absence of GFP expression, and the wild-type sister clones composed of cells that have two copies of GFP (Figure 1B; Supporting Information, Figure S1A–C; File S1).

To assess the effect of $sec5^{ts}$ clones on imaginal disc development, animals were reared at 18° until early third larval instar (L3), 7.5 days AEL, when they were shifted to 30° for 48 hr to ablate the homozygous $sec5^{ts}$ tissue (Figure 1B). Upon shift to 30°, mutant $sec5^{ts}$ cells stained positive for both cleaved caspase and TUNEL and were removed from the epithelium by a combination of basal extrusion and engulfment (Figure 1C; Figure S2A). Despite sustaining significant apoptosis, the resulting adult wings were normally sized (Figure 1, D–F), indicating that the surviving wild-type cells had compensated for the loss of their neighbors. Unlike other methods for inducing imaginal disc damage that cause

a delay in the larval-to-pupal transition presumably to allow adequate time for regeneration (Simpson *et al.* 1980; Stieper *et al.* 2008; Halme *et al.* 2010), *sec5*^{ts}-induced ablation did not significantly delay development (Figure S2B). The absence of a developmental delay indicates that, in this system, the necessary additional growth can occur during a larval stage of normal duration.

The surviving GFP$^+$ tissue in ablated discs must compensate both for the *sec5*^{ts} cells that have been eliminated and for the portion of the posterior compartment that would normally be generated by the proliferation of those cells. Although from the time of upshift until 6 hr after upshift (AUS) ablated and control discs were of comparable size, by 12 hr AUS, ablated discs were significantly smaller than their nonablating counterparts (Figure 1, G and H). Interestingly, this difference was observed for both the posterior and the anterior compartment (Figure S2C), suggesting that, similar to previous reports, damage to the posterior compartment may have a nonautonomous effect on the growth of the rest of the disc (Milan *et al.* 1997; Wells *et al.* 2006; Mesquita *et al.* 2010). Despite being significantly smaller than control discs at 12 hr AUS, ablated discs had largely recovered in size by 36 hr AUS (Figure 1, G and H), suggesting that the surviving GFP$^+$ tissue in ablated discs must grow more rapidly during this time than the GFP$^+$ tissue in control discs. Indeed, although both ablated and control discs started with a GFP$^+$ precursor population of comparable size, this population gave rise to more tissue over the same time period in ablated discs than in controls (Figure 1, G and I). The majority of this extra growth occurred between 12 and 36 hr AUS. During this time, the predicted rate of growth of the GFP$^+$ tissue in ablated discs was at least 1.5 times greater than the rate of growth in control discs (Figure 1I).

Thus, the elimination of patches of *sec5*^{ts} cells from imaginal discs results in the efficient replacement of the lost tissue and the recovery of normally sized adult wings. This recovery is achieved without requiring a developmental delay and it occurs by an increase in the rate of growth of the surviving tissue.

sec5^{ts} *ablation produces compensatory proliferation throughout the affected tissue*

The extra growth induced by *sec5*^{ts} ablation could occur by a localized increase in proliferation adjacent to patches of dying cells, similar to the blastema formed in regenerating discs (Abbott *et al.* 1981; Kiehle and Schubiger 1985; O'Brochta and Bryant 1987; Smith-Bolton *et al.* 2009) or to the nonautonomous proliferation stimulated by undead cells (Huh *et al.* 2004; Perez-Garijo *et al.* 2004; Ryoo *et al.* 2004). Alternatively, it could occur in an apparently asynchronous and diffuse manner throughout the compartment as occurs during normal development (Adler and Macqueen 1984). The latter could be achieved either by an increase in the rate of proliferation of individual cells, or by an increase in the proportion of cells actively dividing, or by a combination of both mechanisms.

As early as 6 hr AUS, ablated discs showed significant levels of apoptosis (Figure 2A). The amount of apoptosis peaked after 12 hr at 30°, and by 36 hr AUS the majority of TUNEL$^+$ puncta marked cellular debris basal to the disc epithelium (Figure 2, B–D; data not shown). At all time points, neither EdU labeling of S-phase cells nor PHH3 labeling of mitotic cells provided consistent evidence for a localized proliferative response to apoptosis (Figure 2, A–D; Figure S3). However, without a decrease in background levels of proliferation, a small localized increase in proliferation might be difficult to detect, particularly if the additional cell cycles were asynchronous.

To determine whether *sec5*^{ts} discs had quantitatively more mitotic cells than control discs, we calculated the density of PHH3$^+$ nuclei (PHH3$^+$ nuclei/1000 pixels area) in the posterior compartment of discs from each population. At 12 hr AUS, ablated discs had a greater density of mitotic cells than controls (Figure 2E), suggesting that a greater proportion of cells were actively dividing. This response occurred shortly after the onset of ablation when levels of apoptosis were the highest. The increase in mitotic cell density may account for the significant recovery in the size of the ablated compartment that we observed between 12 and 24 hr AUS (Figure 1H). Unfortunately we were unable to directly measure proliferation rates, as available methods also rely on clones generated by FLP/FRT mitotic recombination.

At 24 hr AUS, ablated and control discs showed roughly the same density of mitotic cells (Figure 2E). However, in discs dissected from wandering larvae (36–40 hr AUS), the density of mitotic cells declined in control discs while remaining constant in ablated discs (Figure 2E). During normal wing disc development, cell doubling times increase significantly in late discs with most cells eventually arresting in G2 by the end of larval development (Fain and Stevens 1982; Martin *et al.* 2009). Our observations suggest that at least some portion of compensatory growth was accomplished by a delay in this transition to G2 arrest.

Thus we can observe compensatory proliferation at two points during the ablation period. Early compensatory proliferation is coincident with high amounts of apoptosis, although not clearly localized to sites of damage, and occurs concomitantly with the majority of disc size recovery. Late compensatory proliferation occurs after most apoptosis is complete, by an extension of an earlier more rapid growth phase of disc development and may allow ablated discs to fully "catch up" to the size of control discs.

A genetic screen to identify recessive mutations that impair compensatory growth

One strength of the *sec5*^{ts} system is that it allows for unbiased screens using genetic mosaics to find recessive mutations that potentially block compensatory growth. To conduct such a screen, we chose to use the developing eye instead of the wing, since in the adult eye, the proportion

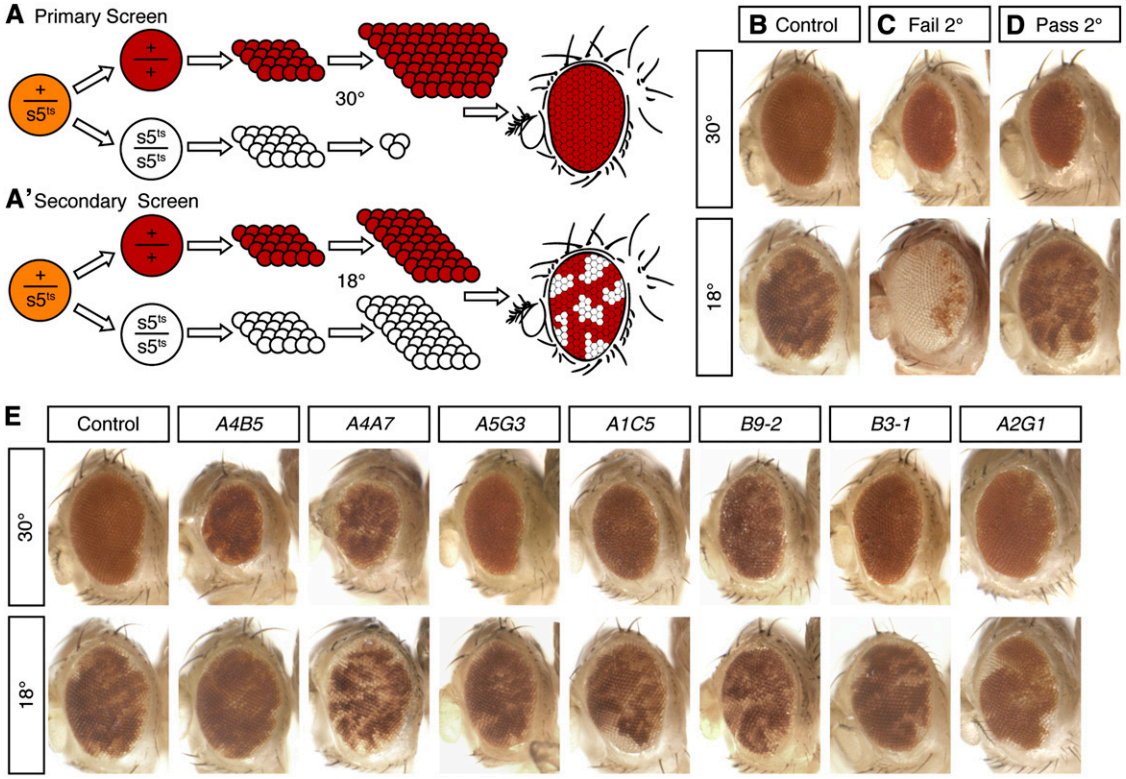

Figure 3 Screen to identify recessive mutations that impair compensatory proliferation. (A and A′) Schematic showing the *sec5*^{ts} system used in the eye. (A) Primary screen: in wild-type animals *sec5*^{ts} ablation resulted in adults with normally sized eyes that were entirely pigmented (red). Mutations that impair developmental or compensatory growth result in a reduced eye. (A′) Secondary screen: in wild-type, nonablated animals, the resulting adults had mosaic eyes composed of wild-type tissue (red) and *sec5*^{ts} tissue (white). Mutations that impair developmental growth result in an underrepresentation of red tissue. (B–D) Examples of phenotypes. (Top) Adult eye following ablation (30°). (Bottom) Adult eye from a nonablated animal (18°). (B) Non-mutagenized parental control phenotype. (C) Mutation that failed the secondary screen and is likely to disrupt normal growth. (D) Mutation that passed the secondary screen and minimally disrupts developmental growth. (E) Representative mutant phenotypes. (Top) Adult eye following ablation (30°). (Bottom) Adult eye from a nonablated animal (18°). Mutants are ordered according to the severity of the phenotype at 30° with the strongest alleles to the left. The parental control phenotype is shown at the far left for comparison.

of wild-type and mutant tissue can be scored easily. This feature is of particular importance when seeking to rule out mutations that merely impair normal growth (see below). To adapt the *sec5*^{ts} system to the eye imaginal disc, we expressed FLP from the *eyeless* (*ey*) promoter, which allowed us to generate discs in which almost all cells were either homozygous for *sec5*^{ts} or wild type (Figure S1, B and C). In addition to being marked by the absence of GFP, *sec5*^{ts} cells also lack a copy of the white gene and lack pigment in the adult eye. When animals are shifted to 30° in the L3 stage of larval development, the resulting adult eyes are normally sized and patterned, but composed largely of red (wild type) tissue (Figure 3, A and B).

If instead, these "red" cells were homozygous for a mutation in a gene required for compensatory growth, they would not be able to compensate for the loss of the "white" tissue at earlier stages of development and the resulting adult eye should be smaller (Figure 3, C and D). However, this assay would not distinguish between mutations that affect developmental growth and those specific to compensatory growth. To attempt to eliminate the former, we conducted a secondary screen in which we generated mosaic eyes, but did not induce ablation of the *sec5*^{ts} tissue. When larvae develop at 18°, adult eyes are mosaic with both white and red tissue present (Figure 3, A′ and B). If a mutation disrupted a gene required for developmental growth, we would expect this to result in the underrepresentation of the red tissue in the adult eye, even in the absence of tissue ablation (Figure 3C). If the effect on developmental growth were minimal, we would expect the amount of red tissue to resemble the nonmutagenized control (Figure 3D).

We performed a screen of the left arm of chromosome 2 (2L), screening ~11,000 individuals each carrying a unique EMS-mutagenized chromosome. Of the 735 mutations initially selected, only 31 were retained after retesting and secondary screening. These 31 mutations fell into 4 two- to three-member lethal complementation groups and 22 putative single hits. The phenotypes ranged from eyes that were less than half the size of control eyes to those that were only slightly reduced in size but rough across the eye (Figures 3E and 4, A and A′). In a few cases, we also observed some variability in the amount of red mutant tissue in animals raised at 18° where tissue ablation does not occur (Figure 3E, *e.g.*, A4A7). Thus a subset of mutations

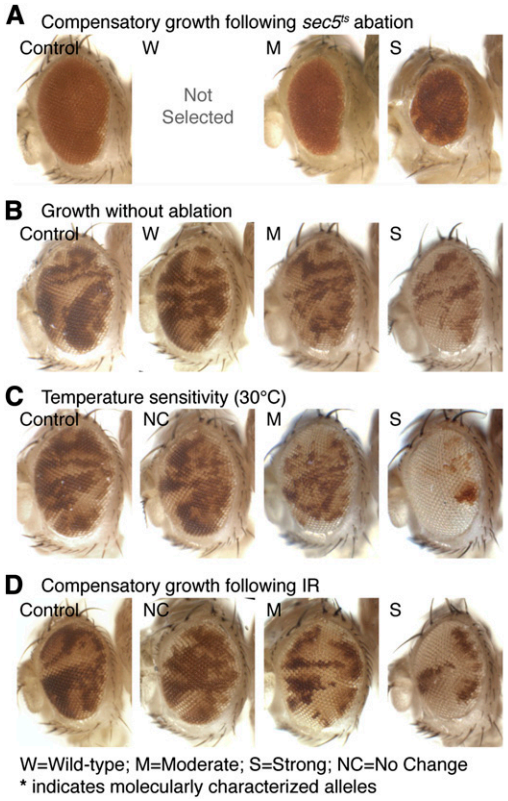

	A'	B'	C'	D'
*A4B5	S	W	NC	NC
*A5G3	M	W	NC	M/S
*B12-3	W/M	W	NC	NC
*B3-1	W/M	W	NC	NC/M
A5D4	M/S	W	NC/M	NC/M
A2G1	W/M	W	NC/M	NC
B12-1	W/M	W	NC/M	NC/M
A2E9	S	W	S	NC/M
*A2I3	M	W/M	NC	NC/M
A2B3	W/M	W/M	NC	NC
A2J5	M	W/M	NC/M	M
A2D1	M/S	W/M	NC/M	M/S
*A1C5	M/S	W/M	M	NC/M
A4F2	M	W/M	M	NC
*A3G1	W/M	W/M	M	NC/M
A5D9	W/M	W/M	M/S	NC/M
A1D3	M	W/M	S	NC
B6-1	S	M	NC	NC
B25-2	M/S	M	NC	M
B18-1	M	M	NC	NC
B7-1	M	M	NC	NC
*B9-2	M	M	NC	M
B18-2	W/M	M	NC	NC
B25-1	M	M	M/S	NC
B6-2	S	M	S	M
B9-1	M/S	M/S	NC	NC/M
*A4A7	M	M/S	NC	NC
A2A3	M/S	M/S	M/S	M
B19-1	S	M/S	S	NC
B-1	S	S	S	—
B12-2	S	S	S	—

Figure 4 Clonal growth assays identify mutations with a temperature- or irradiation-sensitive phenotype. (A and A′) Range of phenotypes following *sec5*^{ts} ablation. Control used for comparison was the parental nonmutagenized phenotype. Animals with a wild-type phenotype were not selected in the screen. (B and B′) Amount of red mutant tissue in adult eye at 25° with no ablation. Control used for comparison was the parental nonmutagenized phenotype. (C and C′) Amount of red mutant tissue in adult eye at 30°. Control used for comparison was the amount of red tissue present for the same genotype at 25°. (D and D′) Amount of red mutant tissue in adult eye following IR-induced ablation. Control used for comparison was the amount of red tissue present for the same genotype in unirradiated samples. Intermediate phenotypes are indicated by W or NC/M and M/S for between W or NC and M and between M and S, respectively. Members of the same lethal complementation group are indicated by colored highlights of the allele name. Genotypes are listed in *Materials and Methods*.

identified in the screen may also subtly compromise developmental growth. However, most of the 31 mutations appeared to fit our initial criteria: a reduction in eye size following ablation and a relatively normal contribution of mutant cells to the adult eye in the absence of ablation.

Our *sec5*^{ts} system required that compensatory growth occur at 30°, while our secondary screen assessed developmental growth at 18°. Thus one important consideration was whether any of our mutations affected normal tissue development at more elevated temperatures. To identify this class of mutant, we generated mosaic eye imaginal discs using a wild-type, nonablating (white) sister clone. We first assessed the amount of red mutant tissue present when animals were raised under standard conditions (25°) as compared to the amount of tissue generated by the nonmutagenized parental chromosome (Figure 4B). We found that 14 of the 31 mutations caused an inferred moderate-to-strong growth defect under these conditions while the remaining 17 did not (Figure 4B′). We then compared the amount of red mutant tissue present at 25° to the amount present if the animals were shifted to 30° during larval development (Figure 4C). Mutants were given a "strong" (S) classification if the amount of red tissue was substantially less at 30° than at 25° (Figure 4C′, *e.g.*, A2E9). If the amount of red tissue was the same at both temperatures, we gave these mutants a "no change" (NC) classification (Figure 4C′, *e.g.*, A4B5). Of the 17 mutants with no obvious growth impairment at 25°, 11 displayed a noticeable growth defect when animals were shifted to 30° (Figure 4C′). In total, when compared to their inferred growth ability at 18°, 25 of the 31 mutations showed a temperature-sensitive phenotype, either at 25° or at 30°.

To circumvent the issue of temperature sensitivity and to assess the impact of these mutations on compensatory proliferation induced by a different type of damage, we used *ey-FLP* to generate mosaic eye imaginal discs and X-ray irradiation (IR) during larval development to stimulate compensatory proliferation. IR causes widespread apoptosis, primarily in actively dividing cells and has been shown to induce a robust compensatory growth response in imaginal discs (Haynie and Bryant 1977; Jaklevic and Su 2004; Halme *et al.* 2010). We compared the amount of red mutant tissue present in unirradiated animals to that found in animals subjected to IR during the early L3 larval stage (Figure 4D). Of the 17

mutations with approximately normal tissue representation in untreated animals, 11 showed a reduction in the amount of red tissue following IR (Figure 4D′). Additionally, another 5 mutants that had a moderate-to-strong underrepresentation of red tissue in untreated animals, showed a further reduction in the amount of red tissue following IR (Figure 4D′). Thus 16 of the 31 mutations identified in our screen may also impede IR-induced compensatory proliferation, suggesting a more general requirement for the affected genes in producing compensatory growth.

The temperature-sensitive growth defect of many of our mutants could be due to a gene product that is inherently unstable at higher temperatures. However, to our knowledge no one has directly assessed the rate of cell division in imaginal discs at different temperatures. As larval development is accelerated at 30°, disc growth may also proceed more rapidly. Thus one reason for the apparent temperature-sensitive phenotype of these mutants could be that they disrupt genes that are limiting for the acceleration of growth. This explanation could also apply to those mutations that showed reduced growth at 25° while appearing normal at 18°, as development proceeds roughly two times faster at 25° than at 18°. We noted that there was substantial overlap between mutations with a temperature-sensitive phenotype and an IR-sensitive one (10 of 15). If indeed both increased temperature and IR-induced damage provoke accelerated growth, these mutations may affect genes that are generally limiting for more rapid growth, such as compensatory proliferation.

Our phenotypic characterization of all mutations recovered from the screen allowed us to set priorities for further study. Of the original 31 mutations, 17 had a minimal effect on growth at 25°. Of these 17, only 6 showed no temperature sensitivity at 30° (*A4B5*, *A5G3*, *B12-3*, *B3-1*, *A2I3*, and *A2B3*). Of these 6, 3 were X-ray sensitive (*A5G3*, *B3-1*, and *A2I3*) and 2 (*B12-3* and *A2I3*) fell into two different lethal complementation groups. (Figure 4). We initially gave highest priority to these 6 mutations with an increased interest in the 3 X-ray–sensitive alleles, as all phenotypic evidence suggested that they might represent a class of genes required specifically for compensatory growth.

However, we also recovered a significant number of mutations that appeared to also be involved in developmental growth. Indeed, although *B12-3* and *A2I3* did not noticeably disrupt normal growth, the second alleles in each complementation group showed a moderate growth defect in the absence of ablation (*A4A7* and *B9-2*, respectively). In this case, *B12-3* and *A2I3* could be hypomorphic alleles capable of providing sufficient gene function for developmental growth but not for more rapid compensatory growth. In a third complementation group (*A1C5/A3G1*), both alleles showed a similar phenotype: a moderate growth defect following *sec5^{ts}* ablation, IR treatment, or shift to 30° and a very mild growth defect at 25° (Figure 4). Although these mutations were unlikely to specifically impact compensatory growth, the possibility that they might represent a class of genes that are required more when growth is accelerated, led us to also pursue their characterization further. We therefore sought to identify the affected genes in our complementation groups by traditional methods and adopted a new approach on the basis of whole genome resequencing to identify the mutated genes in our top candidates, all of which appeared to be single-hit lethal mutations.

Molecular characterization of three lethal complementation groups identified in the screen

Using deficiency mapping and candidate gene sequencing, we were able to find mutations in the *A2I3/B9-2* and *B12-3/A4A7* lethal complementation groups (Figure 5A). In the group composed of *A4A7* and *B12-3*, we identified mutations in *mitochondrial RNA polymerase* (*mtRNApol*). *A4A7*, which showed a stronger phenotype both following *sec5^{ts}* ablation and with respect to growth defects in the absence of ablation, results from a mutation that truncates the protein upstream of the catalytic domain, likely representing a null allele (Figure 5B). *B12-3*, which showed no growth defect in the absence of ablation and weak phenotype following *sec5^{ts}* ablation, causes a glycine-to-glutamic acid substitution in a region of the protein containing no predicted functional domains and is likely to be a weak hypomorph (Figure 5B). Mitochondrial RNA polymerases are required both for transcription of the mitochondrial genome as well as its replication and/or stability. While mutations in *mtRNApol* have not been described previously in *Drosophila*, mutations in the yeast ortholog lead to mitochondrial dysfunction and mutant cells grow more slowly than wild type (Wang and Shadel 1999).

In the group consisting of *B9-2* and *A2I3*, we found mutations in *Topoisomerase3α* (*Top3α*). *Top3α* is a type IA topoisomerase, which is involved in decatenating replicating chromosomes. In *Drosophila*, *Top3α* mutant larvae lack imaginal discs consistent with a mitotic defect (Plank *et al.* 2005). Recent evidence suggests that *Top3α* is also involved in mitochondrial DNA genome maintenance (Wu *et al.* 2010). *A2I3* generates a premature stop truncating the gene product N-terminal to the active site. *B9-2* results from a small deletion within the active site that leads to a frameshift and a premature stop. (Figure 5B). On the basis of the position and nature of our mutations, both are likely to be strong or null alleles. Both alleles showed a robust phenotype following either *sec5^{ts}*- or IR-induced ablation. However, while *B9-2* moderately disrupted developmental growth, *A2I3* had a minimal phenotype under these conditions. Thus *A2I3* may be a slighter weaker allele that more severely compromises compensatory growth, which requires either additional or more rapid cell divisions.

For the third complementation group composed of *A3G1* and *A1C5*, mutations in *CENP-meta* (*cmet*) were identified. *cmet* is a kinetochore kinesin, which is required for maintenance of chromosomes at the metaphase plate, and lack of a functional gene product leads to mitotic abnormalities and cell-cycle arrest (Yucel *et al.* 2000; Maia *et al.* 2007). Both

A

Alleles	Mutation	Gene	Function
B9-2 *A2I3*	115bp deletion K39*	*Top3α*	DNA topoisomerase type 1A
B12-3 *A4A7*	G935E Q807*	*mtRNApol*	mitochondrial RNA polymerase
A1C5 *A3G1*	Q1244* 11bp insertion	*cmet*	kinetochore kinesin

B

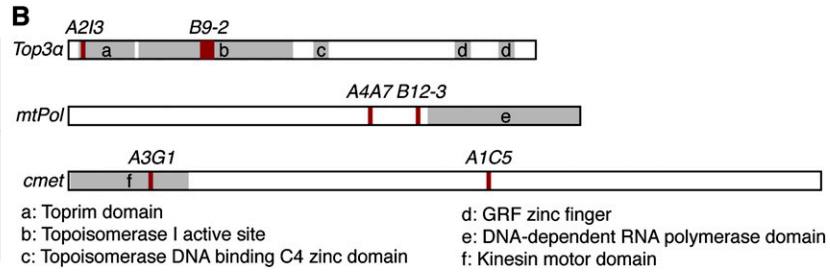

Figure 5 Identification of the affected genes in three complementation groups by deficiency mapping followed by candidate gene sequencing. (A) Three of the lethal complementation groups with allele names, sequenced mutations, affected genes, and gene function. Affected genes were identified by deficiency mapping of the lethal mutation in both members of the complementation group, followed by Sanger sequencing of candidate genes within the lethal interval. (B) Affected genes with the positions of the mutations found marked with respect to predicted functional domains.

alleles introduce premature stop codons: *A3G1*, by a small insertion causing a frameshift within the kinesin motor domain and *A1C5*, by a point mutation further toward the C terminal of the protein (Figure 5B).

Thus, all genes identified in our analysis of the lethal complementation groups appear to be involved in cell growth or cell-cycle progression and are not specifically required for compensatory growth. The recovery of two likely hypomorphic alleles that do not compromise developmental growth suggests that there may be an increased demand for these gene products during compensatory growth.

Characterization of single-hit mutations using WGS

Three mutations, *A4B5*, *A5G3*, and *B3-1*, had no detectable growth defect under normal conditions, but had a consistent and robust phenotype when compensatory growth was induced. Additionally, *B3-1* and *A5G3* showed mild-to-moderate defects following X-ray irradiation (Figure 6A). However, molecular characterization of these mutations was complicated by the fact that these were apparent single hits. Thus mapping the lethal mutation would not necessarily result in the identification of the gene that was causative for the defect in compensatory growth. The advent of massively parallel sequencing technologies has made it feasible to resequence a fly genome rapidly and relatively inexpensively. WGS has been used to identify point mutations in bacteria (Srivatsan *et al.* 2008) and *Caenorhabditis elegans* (Sarin *et al.* 2008). Moreover, recently there has been one successful reported application of WGS to identify an EMS-induced mutation in *Drosophila* (Blumenstiel *et al.* 2009). This encouraged us to identify mutations for each of these three alleles using WGS. Candidate genes could then be followed in recombinant chromosomes to allow for the identification of the mutation relevant to the defect in compensatory proliferation.

In the previous study characterizing an EMS-induced mutation by WGS, flies homozygous for the mutant chromosome were viable. Thus it was possible to generate sequencing libraries from individuals in which the mutation of interest was homozygous. This allowed the authors to set very stringent cutoffs for mutation discovery and to use available software to predict a consensus sequence for both the mutant and parental genotypes. By directly comparing these two consensus assemblies, they were able to identify putative mutations. In contrast, analysis of the mutations identified in our screen was complicated by the fact that each of the mutant chromosomes is homozygous lethal. The necessity of sequencing heterozygous individuals, in combination with the relatively modest levels of genome coverage available with current technologies, required us to modify standard mutation detection software for our purposes. Thus, to identify heterozygous mutations required a different approach to library construction and data analysis than has been used previously.

To identify mutations from heterozygous individuals, we took the following approach. To avoid sequencing non-mutant chromosomes, we crossed each allele to each of the two others to generate three *trans*-heterozygous stocks (Figure 6B). Since each chromosome represented a unique EMS-mutagenized version of the original parental genotype, we reasoned that each *trans*-heterozygous combination would also carry a copy of the wild-type parental allele, thus making sequencing of the parental strain unnecessary. This reduced our sequencing costs significantly. By comparing the mutations found in all three libraries it should, in principle, be possible to assign each mutation to a specific mutant chromosome (Figure 6B). We obtained five- to sevenfold coverage of chromosome 2L for each library (Figure 6D) and mapped all reads to the reference genome using the software MAQ (Li *et al.* 2008).

To analyze our sequencing data, we developed a Perl script that would allow us to extract potential mutations without relying exclusively on MAQ's SNP-calling criteria. Essentially, we generated a list that contained every putative mutation found in our sequencing data as compared to the reference genome. We then used a second customized script to perform a series of pairwise comparisons using the mutation lists for each of our three libraries. For example, we asked for a list of mutations that were present in "ab" and "ac" but not in "bc" to identify polymorphisms unique to "a" or *B3-1* (Figure 6B). By excluding mutations found in bc, we eliminated most polymorphisms between the starting parental chromosome and the reference genome, as these would

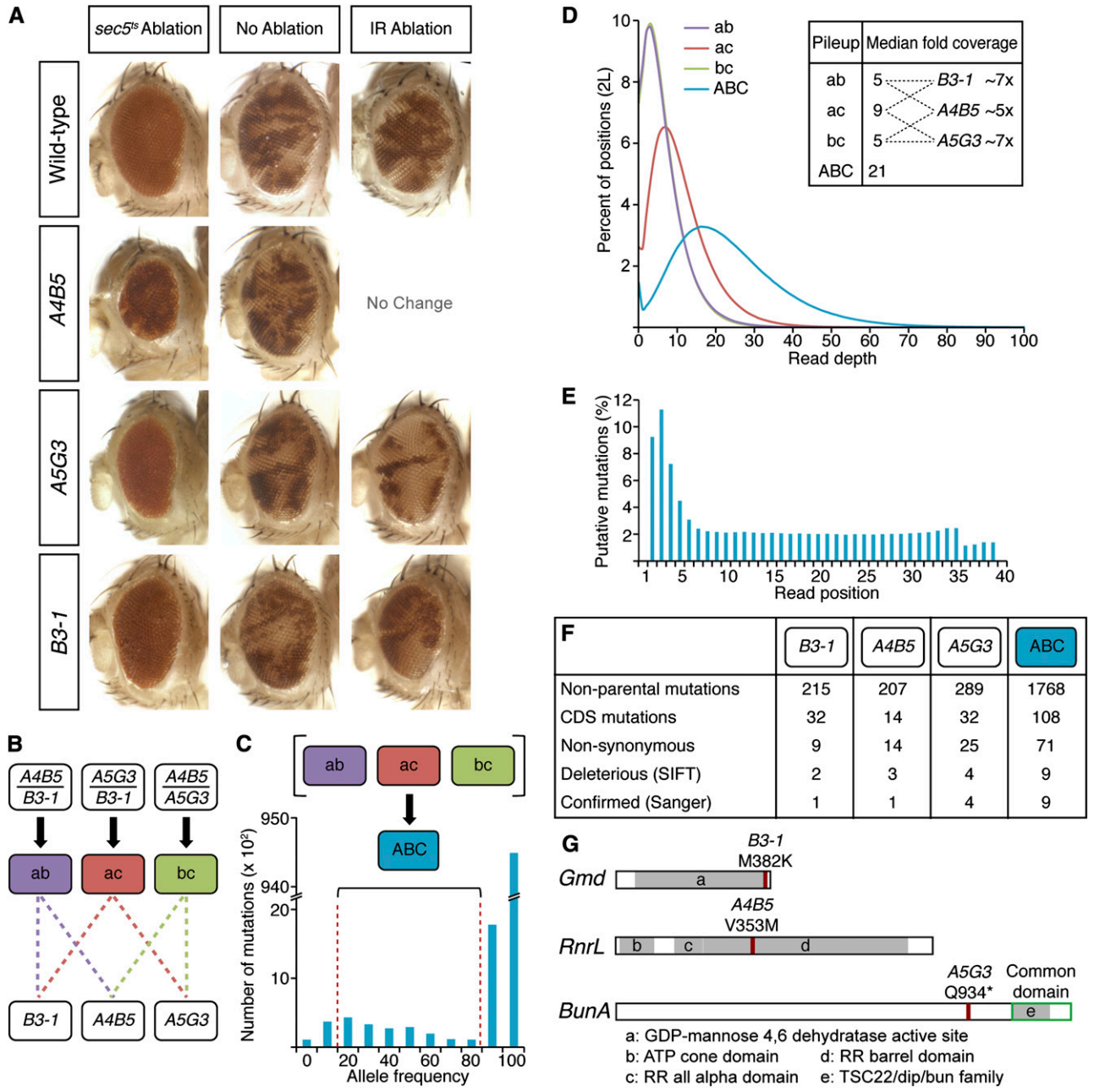

F	B3-1	A4B5	A5G3	ABC
Non-parental mutations	215	207	289	1768
CDS mutations	32	14	32	108
Non-synonymous	9	14	25	71
Deleterious (SIFT)	2	3	4	9
Confirmed (Sanger)	1	1	4	9

Figure 6 Identification of three affected genes by whole-genome resequencing (WGS). (A) Representative phenotypes of the three mutants used for WGS. The phenotypes following *sec5*^{ts} ablation, in nonablated animals raised at 25° and following X-ray irradiation-induced (IR) damage are shown. (B) Scheme showing the genotypes used to generate libraries for WGS and the comparison strategy used to link mutations to a single genotype. (C) Combined data from all genomic libraries (ABC). The distribution of allele frequencies of all mutations and the range selected for analysis is shown. (D) Coverage across 2L was plotted as the percentage of positions on 2L with a given read depth for all four analyses. Inset shows the median coverage for each individual library and the approximate level of coverage for each genotype. The lines for ab and bc are essentially coincident. (E) Disproportionate percentage of mutations was found within the first 5 bases of a read. The percentage of total predicted mutations with a sequencing quality ≥30 was plotted as a function of their read position. (F) Mutation lists were generated as described in *Materials and Methods*. The number of mutations remaining following each refining step is shown. (G) Affected genes with the positions of the mutations found marked with respect to predicted functional domains.

be present in all libraries. By only including mutations present in both ab and ac, we decreased the instance of mutations reported due to mapping or sequencing errors, assuming that the same errors would not be present in both libraries. Finally, we developed a third script that allowed us to search mutations for those occurring specifically in coding sequences. We then refined this list further to include only mutations causing an amino acid change (nonsynonymous mutations) and again to include only nonsynonymous changes that were likely to be deleterious (Figure 6F).

While our comparison strategy using the individual libraries should, at least in theory, provide complete mutation lists for each genotype, our low coverage prompted us to take a second complementary approach. If, for example, a position in ab had insufficient sequencing coverage such that the mutant allele was not represented, we would have excluded this position even if a mutation were found in ac. To address this concern we performed a second analysis by combining all reads from all libraries (Figure 6C). Our combined data gave us 21-fold coverage of chromosome 2L (Figure 6D). Using the same programs mentioned above, we filtered all mutations on the basis of their frequency, excluding very rare or very common mutations as likely to be sequencing errors or parental alleles, respectively (Figure 6C), generating a list of nonsynonymous mutations that was refined further to include only deleterious changes (Figure 6F).

All putative nonsynonymous mutations were examined using Sanger sequencing. We initially found a surprisingly high false positive rate, approaching 90% in some libraries. This appeared to result from an inflated number of mutations called in the first several bases of mapped reads. When we plotted the read position for all mutations with a relatively high sequencing quality, we found that 30% of all mutations were found within bases 2–5 of our reads (Figure 6E). This was not due to a corresponding peak in sequencing quality scores, as these remained relatively constant across reads (Figure S4A). We also did not find a corresponding base composition bias at these early positions (Figure S4B), suggesting that these may not be sequencing errors, but may in fact be changes introduced and then propagated at the end of reads during library construction. To address this issue, we modified our first script to eliminate all mutations found in the first 5 bases of a read. This lowered our false positive rate to <25%, which is reasonable given the absence of a known mutation database to use to train mutation-calling parameters, the low sequencing coverage, and the heterozygous nature of our alleles.

On the basis of our data analysis, we found one candidate mutation in *A4B5*, two in *B3-1*, and six in *A5G3*. *A4B5* had a mutation in *Ribonucleoside diphosphate reductase large subunit* (*RnrL*), while *B3-1* had mutations in *GDP-mannose 4,6-dehydratase* (*Gmd*) and *CG13817*. We outcrossed *B3-1* and *A4B5* to the parental strain for five generations at the end of which lines were reisolated on the basis of the eye phenotype following $sec5^{ts}$-induced ablation. The *A4B5* and *B3-1* chromosomes retained the mutations in *RnrL* and *Gmd*, respectively. In contrast, one line reisolated for *B3-1* had lost the second mutation in *CG13817*. An independently derived allele of *Gmd* also showed the same phenotype following $sec5^{ts}$ ablation (data not shown). *A5G3* had mutations in six genes including *bunched* (*bun*) and *shuttlecraft* (*stc*). The stock was outcrossed to the parental strain and recombinant lines were selected on the basis of separation of *bun* and *stc* from the other four mutations. When retested with the $sec5^{ts}$ system, only the recombinant lines carrying *bun* and *stc* showed the mutant phenotype (data not shown). We did not generate any recombinants between *bun* and *stc*, which are relatively closely linked. While we cannot exclude the possibility that *stc* contributed to the phenotype, independently derived alleles of *bun* (Gluderer *et al.* 2008) showed the same mutant phenotype as *A5G3*. Thus we conclude that the mutant phenotypes of *A4B5*, *B3-1*, and *A5G3* were caused by mutations in *RnrL*, *Gmd*, and *bun*, respectively.

RnrL encodes the large subunit of the ribonucleoside reductase holoenzyme (RR). We found a transition mutation causing a valine-to-methionine substitution at a highly conserved residue within the domain that is predicted to bind the small subunit (*RnrS*) (Figure 6G). RRs catalyze the synthesis of deoxyribonucleotides from their corresponding ribonucleotides and are required to provide dNTPs for DNA synthesis in S phase (Elledge *et al.* 1992). They are also required for recovery following genotoxic stress by maintaining dNTP levels necessary for DNA repair (Tanaka *et al.* 2000).

Gmd is required for the *de novo* synthesis of GDP-fucose, the donor in fucosyltransferease reactions (reviewed in (Becker and Lowe 2003)). As there is no salvage pathway for GDP-fucose synthesis in *Drosophila*, loss of *Gmd* is presumed to block all fucosylation (Roos *et al.* 2002). We identified a transversion mutation that changes a highly conserved methionine to a lysine near the C-terminal end of the *Gmd* active site (Figure 6G).

bun is the *Drosophila* homolog of the mammalian transforming growth factor-β1 stimulated clone 22 (TSC-22), a putative tumor suppressor that is downregulated in several tumor types (Treisman *et al.* 1995; Dobens *et al.* 1997). In the wing disc, *bun* clones were slightly smaller than their wild-type controls, suggesting that *bun* plays a minor role in normal growth (Gluderer *et al.* 2008; Wu *et al.* 2008). Interestingly, *bun* was identified by two independent studies as transcriptionally upregulated in regenerating imaginal discs, suggesting that *bun* may be preferentially required by cells undergoing extra or regenerative growth (Addison *et al.* 1995; Blanco *et al.* 2010). We found a nonsense mutation at glutamine 935, which would result in the premature truncation of the three putative long isoforms of *bun*, bunA, bunF, and bunG and generate a protein lacking the predicted DNA-binding domain (Figure 6G).

The identified mutations represent three putative phenotypic classes

To characterize the phenotypes of $Gmd^{B3\text{-}1}$, $RnrL^{A4B5}$, and bun^{A5G3} further, we tested these alleles in the wing disc $sec5^{ts}$ ablation system (Figure 1A). All three alleles showed a reduced-wing phenotype (Figure 7, A–D), suggesting that, as in the eye, mutation of any of these genes reduces compensatory growth in the wing. These effects cannot be attributed to an acceleration of development, which would be predicted to impair compensatory growth since imaginal discs from older larvae are less capable of regeneration

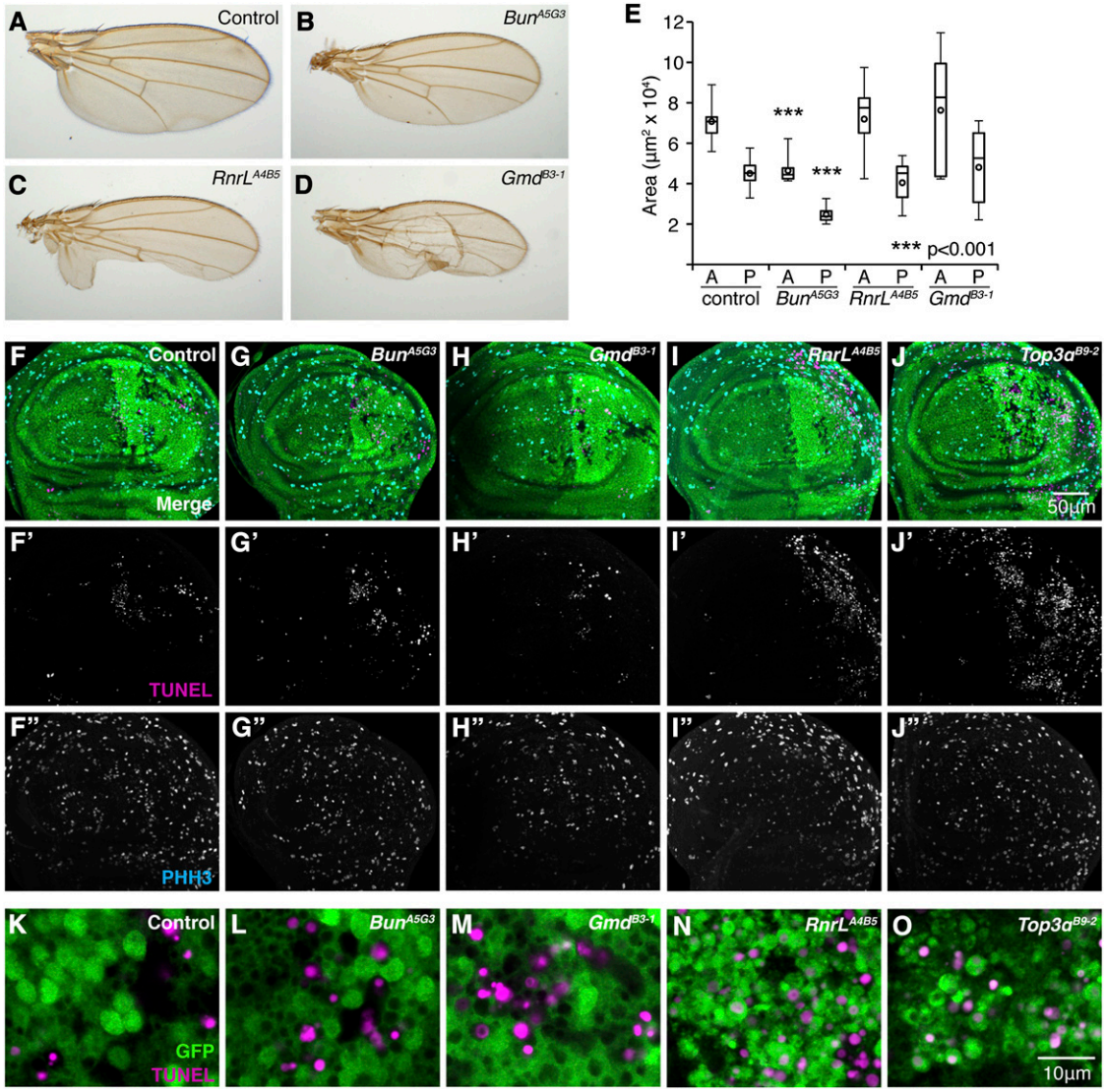

Figure 7 Identified mutants fell into three putative phenotypic classes. (A–D) The resulting adult wings after *sec5*^{ts} ablation for *bun*^{A5G3} (B) *RnrL*^{A4B5} (C), and *Gmd*$^{B3\text{-}1}$ (D) all show size defects as compared to control (A). (B) Only *bun*^{A5G3} mutant discs were smaller than controls at the end of the ablation period. Quantification of wing disc area, anterior and posterior compartments, 48 hr AUS, comparing the size of mutant discs to the control. (F–J) Wing imaginal discs dissected at 48 hr AUS and stained with PHH3 (cyan) to mark mitotic cells and TUNEL (magenta) to mark apoptotic cells. For PHH3 and TUNEL, images are *z*-max projections of confocal slices through the entire disc epithelium. For GFP, images are a single confocal slice. Posterior is to the left. (F–F′′) Parental control disc. Minimal TUNEL$^+$ cells remain and PHH3$^+$ cells are evident particularly in the posterior compartment. (G–G′′) *bun*^{A5G3} discs are noticeably smaller, but TUNEL staining is comparable to the control and proliferation is evident. (H–H′′) *Gmd*$^{B3\text{-}1}$ discs are indistinguishable from parental controls. (I–I′′) *RnrL*^{A4B5} discs are comparable in size to parental controls, but have high levels of apoptosis in the posterior compartment. Mitotic cells are still evident in the posterior compartment (J–J′′) *Top3α*$^{B9\text{-}2}$ discs show a similar phenotype to *RnrL*^{A4B5} discs. (K–O) High magnification images showing both TUNEL (magenta) and GFP (green). Single confocal sections through the basal portion of the disc epithelium are shown. Residual apoptotic cells in control (K), *bun*^{A5G3} (L), and *Gmd*$^{B3\text{-}1}$ (M) discs are largely GFP$^-$. Additional apoptotic cells in *RnrL*^{A4B5} (N) and *Top3α*$^{B9\text{-}2}$ (O) discs are mostly GFP$^+$ (*i.e.*, mutant for *RnrL*^{A4B5} or *Top3α*$^{B9\text{-}2}$).

(Figure S5). At the end of the ablation period (48 hr AUS), we found that only discs in which the compensating cells were mutant for *bun*^{A5G3} was disc size strongly affected (Figure 7E). This reduction in size was observed in both the posterior and anterior compartment. We did not observe elevated levels of apoptosis in the posterior compartment and mitoses were still evident (Figure 7, G and L), suggesting that *bun*^{A5G3} mutant cells were viable and still capable of proliferating. The disc and adult wing phenotype of *bun*^{A5G3} suggest that *bun* may be required to initiate and/or sustain compensatory growth.

Although both *Gmd*$^{B3\text{-}1}$and *RnrL*^{A4B5} caused substantial defects in the resulting adult wings (Figure 7, C and D), at 48 hr AUS wing imaginal discs from these animals were not correspondingly reduced in size (Figure 7E). Discs in which the compensating cells were *Gmd*$^{B3\text{-}1}$ showed no obvious abnormalities, suggesting that the loss of *Gmd* does not impact the ability of disc cells to undergo compensatory

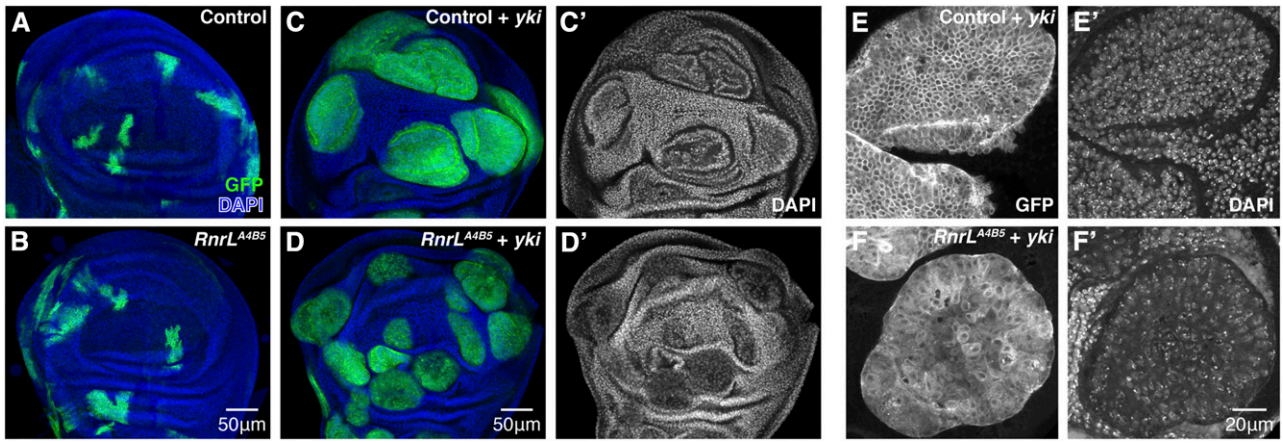

Figure 8 *RnrL*^{A4B5} partially suppressed overgrowth induced by overexpression of activated Yorkie. (A–D) Wing imaginal discs with MARCM clones shown in green (GFP) and nuclei (DAPI) in blue. Bar, 50 μm. (A and B) *RnrL*^{A4B5} mutant clones were comparable in size to control clones. Wing imaginal discs with MARCM clones in which GFP$^+$ cells (green) were homozygous for either the parental control chromosome (A) or *RnrL*^{A4B5} (B). (C and D) *RnrL*^{A4B5} mutant clones overexpressing activated *yorkie* (*yki*) were noticeably smaller than control clones and stained weakly for DAPI. MARCM clones in which GFP$^+$ cells (green) were overexpressing activated *yki* and were homozygous for either the parental control chromosome (C) or *RnrL*^{A4B5} (D). DAPI is shown in white for control (C′) and *RnrL*^{A4B5} (D′) discs. Single confocal sections are shown. (E and F) Clones overexpressing activated *yki* and mutant for *RnrL*^{A4B5} appear to have fewer and larger cells than controls. High magnification images of single clones homozygous for the parental control (E) or *RnrL*^{A4B5} (F) and overexpressing activated *yki*. mCD8-GFP marks the cell membrane (E and F) and DAPI marks nuclei (E′ and F′).

growth and that *Gmd* may be required later during pupal wing development (Figure 7, H and M). Indeed, the most common defect observed in the adult wings of these animals is blistering (Figure 7D), which is often caused by faulty adhesion between the dorsal and ventral wing surface.

Discs in which the compensating cells were *RnrL*^{A4B5} were similar in size to discs with wild-type cells (Figure 7E). However, the posterior compartment showed very high levels of apoptotic cells (Figure 7, I and N). These dying cells were not residual *sec5*^{ts} cells, but were largely GFP$^+$ and hence homozygous for *RnrL*^{A4B5} (Figure 7N). Despite high levels of apoptosis, mitotic cells are still evident in the posterior compartment (Figure 7I′′). Thus cells with reduced RnrL function may be initially capable of engaging in compensatory growth and generating a fairly normally sized posterior compartment, but these cells are sensitized to apoptosis. Lack of *RnrL* would reduce the amount of dNTPs available for DNA replication (Elledge *et al.* 1992). Increased proliferation when DNA replication is compromised can result in high levels of apoptosis (Sampath *et al.* 2003). Loss of *Top3α* might impair disentanglement of replicated DNA (Plank *et al.* 2005) and could therefore have a similar effect. Indeed when we examined discs containing clones of one of the *Top3α* alleles identified in the screen, we found similarly high levels of apoptosis (Figure 7, J and O).

Loss of RnrL partially inhibits Yorkie-induced tissue overgrowth

RnrL did not obviously impair growth in imaginal discs under normal conditions but did compromise compensatory growth. Given the reported function of RRs in dNTP and thus DNA synthesis, it is surprising that a mutation in *RnrL* would not cause a general growth defect. A likely explanation is that *RnrL*^{A4B5}, and potentially other mutations like it, may provide a sufficient threshold of gene function for normal growth, but that increased demand for gene activity in rapidly dividing cells would result in a preferential inhibition of compensatory growth. If true, we might expect loss of *RnrL* to also curtail tissue overgrowth that can be induced by a variety of genetic changes. To test this possibility, we used the MARCM method to examine the effect of mutation of *RnrL* on clones of cells that overexpress an activated form of *yorkie* (*yki*) (Oh and Irvine 2008). The Yorkie protein is a potent stimulator of tissue growth in imaginal discs and increased levels of the mammalian ortholog of Yki, YAP, are found in several human cancers (Huang *et al.* 2005).

While MARCM clones that were solely mutant for *RnrL*^{A4B5} were indistinguishable from control clones of the parental gentoype (Figure 8, A and B), an obvious difference was observed when these clones were also overexpressing *yki*. *RnrL*^{A4B5}, *UAS-yki* clones were smaller than parental, *UAS-yki* clones (Figure 8, C and D). In addition, the nuclear density appeared to be decreased in some *RnrL*^{A4B5}, *UAS-yki* clones and cell size increased (Figure 8, E and F), suggesting that cell growth and cell-cycle progression may have become uncoupled. The ability of *RnrL*^{A4B5} to partially block *yki*-induced overgrowth suggests that wild-type levels of *RnrL* function are especially necessary for more rapidly dividing cells. Thus a subset of mutations that compromise compensatory growth may also limit tissue overgrowth.

Discussion

Genetic screens in *Drosophila*, and mosaic screens in particular, are a proven means for dissecting biological processes of interest, identifying novel genes and uncovering new

roles for known genes. We have developed a system that allows us to apply the power of *Drosophila* genetics to address the question of how compensatory growth is generated and regulated. We were able to conditionally ablate patches of cells within the developing imaginal disc by generating mosaic tissues in which one population of cells carried a recessive temperature-sensitive cell-lethal mutation. We could then assay the ability of the surviving reciprocal clones to compensate for the tissue loss both by looking at features of the disc itself and by assessing the size of resulting adult structure. By developing a mosaic system, we were able to screen for recessive mutations that would disrupt this process.

Characterization of our system revealed that *sec5^{ts}* ablation did not induce blastema formation. Rather imaginal disc recovery occurred by compensatory proliferation in two stages. At early stages when levels of apoptosis were highest, ablating discs had a greater proportion of mitotic cells than control discs, suggesting that damage may directly promote additional proliferation. If surviving cells were responding directly to dying cells, it would suggest the existence of a regulatory mechanism distinct from those that are employed during normal disc development. However, unlike the nonautonomous proliferation induced by undead cells, we found no clear evidence that the increased proliferation is localized adjacent to the deleted tissue. In addition, at late stages, when normal growth in control discs slowed, ablated discs continued to show levels of proliferation comparable to slightly younger discs. As the amount of apoptosis in ablated discs was relatively low at this time, this late growth is unlikely to occur in direct response to damaged tissue. Thus compensatory growth may be a broader tissuewide response. As such, it may be regulated by the same patterning and size-sensing mechanisms that function during normal development (Mesquita *et al.* 2010).

We conducted a screen for recessive mutations that block compensatory growth. Three of the mutations that we identified as being most likely to specifically affect compensatory growth were found to disrupt the genes *bun*, *Gmd*, and *RnrL*. Our data indicate that *bun* is required to produce a normal amount of compensatory growth. The normal biological function of *bun* and its mammalian ortholog TSC-22 are still poorly understood. In *Drosophila*, overexpression of BunA alone has no effect on imaginal disc growth (Gluderer *et al.* 2008). However, coexpression with Madm, a protein with a catalytically inactive kinase-like domain that can bind to BunA, results in increased growth of imaginal discs (Gluderer *et al.* 2010). Mutant forms of *bun* have been shown to have a subtle effect on growth under normal conditions. Clones of cells lacking the long isoform of *bun* (*bunA*) display, at best, mild growth defects in imaginal discs. However, eye imaginal discs that are composed almost entirely of mutant *bun* cells, develop into adult eyes composed of both fewer and smaller cells (Gluderer *et al.* 2008). These discs were generated by mitotic recombination with a chromosome bearing a cell-lethal mutation and therefore produce a situation not all that dissimilar to our *sec5^{ts}* ablation system. Additionally, *bun* has been shown to be upregulated in imaginal discs undergoing regeneration after either surgical or genetic ablation of a portion of the disc (Addison *et al.* 1995; Blanco *et al.* 2010). Taken together with our findings, these observations implicate *bun* in the regulation of both regenerative and compensatory growth.

The mechanisms by which *bun* regulates growth are not known. Since *bun* encodes a protein that has a leucine zipper as well as a TSC box that appears capable of binding DNA *in vitro*, it was initially assumed that it functions as a transcriptional regulator. More recent studies have shown that Bun and Madm colocalize to the Golgi in S2 cells (Gluderer *et al.* 2010) and that knockdown of Madm by RNAi interferes with protein secretion (Bard *et al.* 2006). Since both the expression and requirement for Bun seem to be increased when regenerative or compensatory growth are required, future of studies of Bun in this biological context may provide more mechanistic insights into Bun function.

Imaginal discs in which the compensating cells were *Gmd$^{B3\text{-}1}$* recovered in size following ablation but were still unable to produce a morphologically normal adult structure. This suggests that *Gmd* may be more important for tissue patterning or morphogenesis following ablation than for compensatory growth *per se*. In *Drosophila*, *Gmd* has been studied primarily in the context of Notch signaling, where loss of *Gmd* blocks expression of Notch target genes and results in reduced growth of the wing disc (Okajima *et al.* 2005). However, when this observation was tested by clonal analysis, rather than in homozygous mutant animals, *Gmd* clones did not have an obvious phenotype. Only when very large *Gmd* clones were generated was loss of the Notch target Wingless observed and only at sites distant from any wild-type cells, suggesting that the requirement for *Gmd* may not be cell autonomous (Okajima *et al.* 2008). We did not observe defects in the expression of the Notch target Wingless even when the majority of the posterior compartment was composed of *Gmd$^{B3\text{-}1}$* mutant cells (data not shown), suggesting that the defects that we observed in ablated adult structures were not a consequence of reduced Notch activity in the larval disc. Fucosylation is also necessary for the formation of many different glycan structures that modulate the activity of a variety of proteins, including signaling and cell adhesion molecules, one or many of which may participate in disc patterning and morphogenesis.

Reducing *RnrL* function did not reduce compensatory growth as mutant cells were able to generate a normally sized posterior compartment; rather, mutant cells engaged in compensatory growth appeared to be predisposed to apoptosis. In *Drosophila*, no mutant phenotype has been characterized at the cellular level for either *RnrL* or *RnrS*. However, *RnrL* transcription is induced at the G1-to-S transition by E2F and is presumably required for DNA synthesis (Duronio and O'Farrell 1994). Thus compromising *RnrL* function may render cells incapable of increasing their rate of cell-cycle progression to keep pace with the increased rate of tissue growth required

following tissue ablation. Consistent with this possibility is our observation that *RnrL*^{A4B5} restricts the growth of clones that overexpress an activated form of Yki and that the growth of these cells appears to have outpaced their rate of division. Interestingly increased RR activity is associated with many malignant cancers, indicating that an increase in RR activity may be required to sustain increased levels of cell proliferation. Consistent with this, RRs are the targets of several common chemotherapeutic agents used in cancer treatment (Shao *et al.* 2006). Together, these observations suggest that some similarities may exist between compensatory growth and hyperplastic overgrowth.

Our findings also indicate that some of the differences between compensatory growth and normal growth are likely to be quantitative rather than qualitative. The *RnrL* allele that we identified may be hypomorphic and more severe alleles may perturb normal growth. When we identified the causative mutations in three of the complementation groups found in our screen, each disrupted a gene that likely functions during cell growth or proliferation under normal conditions, yet the requirement for these genes appears to be enhanced when additional growth is required. Interestingly, we identified mutations in *Top3α* as strongly disrupting both *sec5*^{ts}- and IR-induced compensatory growth. Topoisomerases are chemotherapeutic targets and topoisomerase IIα was recently shown to be haploinsufficient for liver regeneration in zebrafish, suggesting that abnormally proliferating cells may be particularly sensitive to the loss of topoisomerase activity (Damelin and Bestor 2007; Dovey *et al.* 2009). Our screen may therefore have enriched for a set of mutations that reduce gene function to a level that is near the threshold required for developmental growth and is insufficient for compensatory growth, which requires either additional or more rapid cell divisions. These findings reinforce the idea that compensatory growth is intimately connected to developmental growth, but might place an increased demand on certain pathways that sustain normal cellular requirements for cell-cycle progression and growth.

Our results also validate the approach of identifying EMS-induced mutations by whole-genome resequencing. In the one previous case where this strategy has been applied successfully in *Drosophila*, it was possible to distinguish genuine mutations from those that arose during library construction or sequencing by looking for those that had a high allele frequency (Blumenstiel *et al.* 2009). Unfortunately their approach is not suitable for situations where mutations are homozygous lethal. We therefore developed a method of library construction and computational analysis that is generally applicable to mutations that are homozygous lethal and we have used it successfully to identify three of the mutations generated in our screen. Moreover, our programs have also been used more recently to identify chemically induced mutations in *C. elegans* (D. Richter, unpublished data).

Finally, we have shown that the system that we have developed for studying compensatory growth is indeed capable of generating and characterizing mutations that, at least to some extent, impair compensatory growth more than normal growth. The issue of whether there are genes that are required exclusively for compensatory growth is still unresolved. However, using this system and others like it, it will be possible to conduct more extensive genetic screens for mutations that influence compensatory growth or regeneration. The system that we have used can be extended in two ways. First, by engineering fly lines in which transposon insertions on each of the chromosome arms carry a wild-type copy of the *sec5* gene in a *sec5*^{ts} background, it should be possible to screen most of the genome. Second, by targeting FLP to a variety of tissues, it should be possible to investigate the capacity of each of those tissues for compensatory growth.

Acknowledgments

We are grateful to Thomas Schwarz for generously providing the *sec5*^{ts1} allele used in this study long before it was published and to Adrian Halme for initial experiments establishing the feasibility of using *sec5*^{ts} for ablating portions of imaginal discs. We thank Leath Tonkin and the Vincent J. Coates Genomics Sequencing Laboratory for sequencing data and helpful discussion regarding library construction. We also thank Sarah Siegrist and Karsten Siller for comments on this manuscript. This research was supported by grant RO1GM085576 from the National Institutes of Health and an American Cancer Society research professor award 120366-RP-11-078-01-DDC to I.K.H. and a National Science Foundation graduate research fellowship to A.R.G.

Literature Cited

Abbott, L. C., G. H. Karpen, and G. Schubiger, 1981 Compartmental restrictions and blastema formation during pattern regulation in Drosophila imaginal leg discs. Dev. Biol. 87: 64–75.

Addison, W. R., W. J. Brook, L. D. Querengesser, S. Y. Tiong, and M. A. Russell, 1995 Analysis of an enhancer trap expressed in regenerating Drosophila imaginal discs. Genome 38: 724–736.

Adler, P. N., and M. MacQueen, 1984 Cell proliferation and DNA replication in the imaginal wing disc of Drosophila melanogaster. Dev. Biol. 103: 28–37.

Bard, F., L. Casano, A. Mallabiabarrena, E. Wallace, K. Saito *et al.*, 2006 Functional genomics reveals genes involved in protein secretion and Golgi organization. Nature 439: 604–607.

Becker, D. J., and J. B. Lowe, 2003 Fucose: biosynthesis and biological function in mammals. Glycobiology 13: 41R–53R.

Bergmann, A., and H. Steller, 2010 Apoptosis, stem cells, and tissue regeneration. Sci. Signal. 3: re8.

Blair, S. S., 1992 Engrailed expression in the anterior lineage compartment of the developing wing blade of Drosophila. Development 115: 21–33.

Blanco, E., M. Ruiz-Romero, S. Beltran, M. Bosch, A. Punset *et al.*, 2010 Gene expression following induction of regeneration in Drosophila wing imaginal discs. Expression profile of regenerating wing discs. BMC Dev. Biol. 10: 94.

Blumenstiel, J. P., A. C. Noll, J. A. Griffiths, A. G. Perera, K. N. Walton *et al.*, 2009 Identification of EMS-induced mutations

in *Drosophila melanogaster* by whole-genome sequencing. Genetics 182: 25–32.
Brockes, J. P., and A. Kumar, 2008 Comparative aspects of animal regeneration. Annu. Rev. Cell Dev. Biol. 24: 525–549.
Bryant, P. J., and P. Simpson, 1984 Intrinsic and extrinsic control of growth in developing organs. Q. Rev. Biol. 59: 387–415.
Chera, S., L. Ghila, K. Dobretz, Y. Wenger, C. Bauer *et al.*, 2009 Apoptotic cells provide an unexpected source of Wnt3 signaling to drive hydra head regeneration. Dev. Cell 17: 279–289.
Conlon, I., and M. Raff, 1999 Size control in animal development. Cell 96: 235–244.
Damelin, M., and T. H. Bestor, 2007 The decatenation checkpoint. Br. J. Cancer 96: 201–205.
Dobens, L. L., T. Hsu, V. Twombly, W. M. Gelbart, L. A. Raftery *et al.*, 1997 The Drosophila bunched gene is a homologue of the growth factor stimulated mammalian TSC-22 sequence and is required during oogenesis. Mech. Dev. 65: 197–208.
Dovey, M., E. E. Patton, T. Bowman, T. North, W. Goessling *et al.*, 2009 Topoisomerase II alpha is required for embryonic development and liver regeneration in zebrafish. Mol. Cell. Biol. 29: 3746–3753.
Duronio, R. J., and P. H. O'Farrell, 1994 Developmental control of a G1-S transcriptional program in Drosophila. Development 120: 1503–1515.
Elledge, S. J., Z. Zhou, and J. B. Allen, 1992 Ribonucleotide reductase: regulation, regulation, regulation. Trends Biochem. Sci. 17: 119–123.
Fain, M. J., and B. Stevens, 1982 Alterations in the cell cycle of Drosophila imaginal disc cells precede metamorphosis. Dev. Biol. 92: 247–258.
Fan, Y., and A. Bergmann, 2008 Apoptosis-induced compensatory proliferation. The Cell is dead. Long live the Cell! Trends Cell Biol. 18: 467–473.
Gluderer, S., S. Oldham, F. Rintelen, A. Sulzer, C. Schutt *et al.*, 2008 Bunched, the Drosophila homolog of the mammalian tumor suppressor TSC-22, promotes cellular growth. BMC Dev. Biol. 8: 10.
Gluderer, S., E. Brunner, M. Germann, V. Jovaisaite, C. Li *et al.*, 2010 Madm (Mlf1 adapter molecule) cooperates with Bunched A to promote growth in Drosophila. J. Biol. 9: 9.
Hadorn, E., and D. Buck, 1962 On the differentiation of transplanted wing imaginal disc fragments of Drosophila melanogaster. Rev. Suisse Zool. 69: 302–310 (in German).
Halme, A., M. Cheng, and I. K. Hariharan, 2010 Retinoids regulate a developmental checkpoint for tissue regeneration in Drosophila. Curr. Biol. 20: 458–463.
Haynie, J. L., and P. J. Bryant, 1977 The effects of X-rays on the proliferation dynamics of cells in the imaginal disc of Drosophila melanogaster. Rouxs Arch. Dev. Biol. 183: 85–100.
Huang, J., S. Wu, J. Barrera, K. Matthews, and D. Pan, 2005 The Hippo signaling pathway coordinately regulates cell proliferation and apoptosis by inactivating Yorkie, the Drosophila homolog of YAP. Cell 122: 421–434.
Huh, J. R., M. Guo, and B. A. Hay, 2004 Compensatory proliferation induced by cell death in the Drosophila wing disc requires activity of the apical cell death caspase Dronc in a nonapoptotic role. Curr. Biol. 14: 1262–1266.
Jaklevic, B. R., and T. T. Su, 2004 Relative contribution of DNA repair, cell cycle checkpoints, and cell death to survival after DNA damage in Drosophila larvae. Curr. Biol. 14: 23–32.
Kiehle, C. P., and G. Schubiger, 1985 Cell proliferation changes during pattern regulation in imaginal leg discs of Drosophila melanogaster. Dev. Biol. 109: 336–346.
Kumar, P., S. Henikoff, and P. C. Ng, 2009 Predicting the effects of coding non-synonymous variants on protein function using the SIFT algorithm. Nat. Protoc. 4: 1073–1081.
Langevin, J., M. J. Morgan, J. B. Sibarita, S. Aresta, M. Murthy *et al.*, 2005 Drosophila exocyst components Sec5, Sec6, and Sec15 regulate DE-Cadherin trafficking from recycling endosomes to the plasma membrane. Dev. Cell 9: 365–376.
Li, H., J. Ruan, and R. Durbin, 2008 Mapping short DNA sequencing reads and calling variants using mapping quality scores. Genome Res. 18: 1851–1858.
Maia, A. F., C. S. Lopes, and C. E. Sunkel, 2007 BubR1 and CENP-E have antagonistic effects upon the stability of microtubule-kinetochore attachments in Drosophila S2 cell mitosis. Cell Cycle 6: 1367–1378.
Martin, F. A., S. C. Herrera, and G. Morata, 2009 Cell competition, growth and size control in the Drosophila wing imaginal disc. Development 136: 3747–3756.
Mesquita, D., A. Dekanty, and M. Milan, 2010 A dp53-dependent mechanism involved in coordinating tissue growth in Drosophila. PLoS Biol. 8: e1000566.
Milan, M., S. Campuzano, and A. Garcia-Bellido, 1997 Developmental parameters of cell death in the wing disc of *Drosophila*. Proc. Natl. Acad. Sci. USA 94: 5691–5696.
Murthy, M., R. O. Teodoro, T. P. Miller, and T. L. Schwarz, 2010 Sec5, a member of the exocyst complex, mediates Drosophila embryo cellularization. Development 137: 2773–2783.
O'Brochta, D. A., and P. J. Bryant, 1987 Distribution of S-phase cells during the regeneration of Drosophila imaginal wing discs. Dev. Biol. 119: 137–142.
Oh, H., and K. D. Irvine, 2008 In vivo regulation of Yorkie phosphorylation and localization. Development 135: 1081–1088.
Okajima, T., A. Xu, L. Lei, and K. D. Irvine, 2005 Chaperone activity of protein O-fucosyltransferase 1 promotes notch receptor folding. Science 307: 1599–1603.
Okajima, T., B. Reddy, T. Matsuda, and K. D. Irvine, 2008 Contributions of chaperone and glycosyltransferase activities of O-fucosyltransferase 1 to Notch signaling. BMC Biol. 6: 1.
Pellettieri, J., P. Fitzgerald, S. Watanabe, J. Mancuso, D. R. Green *et al.*, 2010 Cell death and tissue remodeling in planarian regeneration. Dev. Biol. 338: 76–85.
Perez-Garijo, A., F. A. Martin, and G. Morata, 2004 Caspase inhibition during apoptosis causes abnormal signalling and developmental aberrations in Drosophila. Development 131: 5591–5598.
Perez-Garijo, A., E. Shlevkov, and G. Morata, 2009 The role of Dpp and Wg in compensatory proliferation and in the formation of hyperplastic overgrowths caused by apoptotic cells in the Drosophila wing disc. Development 136: 1169–1177.
Plank, J. L., S. H. Chu, J. R. Pohlhaus, T. Wilson-Sali, and T. S. Hsieh, 2005 Drosophila melanogaster topoisomerase IIIalpha preferentially relaxes a positively or negatively supercoiled bubble substrate and is essential during development. J. Biol. Chem. 280: 3564–3573.
Roos, C., M. Kolmer, P. Mattila, and R. Renkonen, 2002 Composition of Drosophila melanogaster proteome involved in fucosylated glycan metabolism. J. Biol. Chem. 277: 3168–3175.
Ryoo, H. D., T. Gorenc, and H. Steller, 2004 Apoptotic cells can induce compensatory cell proliferation through the JNK and the Wingless signaling pathways. Dev. Cell 7: 491–501.
Sampath, D., V. A. Rao, and W. Plunkett, 2003 Mechanisms of apoptosis induction by nucleoside analogs. Oncogene 22: 9063–9074.
Sarin, S., S. Prabhu, M. M. O'Meara, I. Pe'er, and O. Hobert, 2008 Caenorhabditis elegans mutant allele identification by whole-genome sequencing. Nat. Methods 5: 865–867.
Shao, J., B. Zhou, B. Chu, and Y. Yen, 2006 Ribonucleotide reductase inhibitors and future drug design. Curr. Cancer Drug Targets 6: 409–431.

Simpson, P., P. Berreur, and J. Berreur-Bonnenfant, 1980 The initiation of pupariation in Drosophila: dependence on growth of the imaginal discs. J. Embryol. Exp. Morphol. 57: 155–165.

Smith-Bolton, R. K., M. I. Worley, H. Kanda, and I. K. Hariharan, 2009 Regenerative growth in Drosophila imaginal discs is regulated by Wingless and Myc. Dev. Cell 16: 797–809.

Srivatsan, A., Y. Han, J. Peng, A. K. Tehranchi, R. Gibbs *et al.*, 2008 High-precision, whole-genome sequencing of laboratory strains facilitates genetic studies. PLoS Genet. 4: e1000139.

St Johnston, D., 2002 The art and design of genetic screens: Drosophila melanogaster. Nat. Rev. Genet. 3: 176–188.

Stieper, B. C., M. Kupershtok, M. V. Driscoll, and A. W. Shingleton, 2008 Imaginal discs regulate developmental timing in Drosophila melanogaster. Dev. Biol. 321: 18–26.

Stoick-Cooper, C. L., R. T. Moon, and G. Weidinger, 2007 Advances in signaling in vertebrate regeneration as a prelude to regenerative medicine. Genes Dev. 21: 1292–1315.

Tanaka, H., H. Arakawa, T. Yamaguchi, K. Shiraishi, S. Fukuda *et al.*, 2000 A ribonucleotide reductase gene involved in a p53-dependent cell-cycle checkpoint for DNA damage. Nature 404: 42–49.

Treisman, J. E., Z. C. Lai, and G. M. Rubin, 1995 Shortsighted acts in the decapentaplegic pathway in Drosophila eye development and has homology to a mouse TGF-beta-responsive gene. Development 121: 2835–2845.

Tseng, A. S., D. S. Adams, D. Qiu, P. Koustubhan, and M. Levin, 2007 Apoptosis is required during early stages of tail regeneration in Xenopus laevis. Dev. Biol. 301: 62–69.

Wang, Y., and G. S. Shadel, 1999 Stability of the mitochondrial genome requires an amino-terminal domain of yeast mitochondrial RNA polymerase. Proc. Natl. Acad. Sci. USA 96: 8046–8051.

Wells, B. S., E. Yoshida, and L. A. Johnston, 2006 Compensatory proliferation in Drosophila imaginal discs requires Dronc-dependent p53 activity. Curr. Biol. 16: 1606–1615.

Wu, J., L. Feng, and T. S. Hsieh, 2010 *Drosophila* topo IIIalpha is required for the maintenance of mitochondrial genome and male germ-line stem cells. Proc. Natl. Acad. Sci. USA 107: 6228–6233.

Wu, J. S., and L. Luo, 2006 A protocol for mosaic analysis with a repressible cell marker (MARCM) in Drosophila. Nat. Protoc. 1: 2583–2589.

Wu, X., M. Yamada-Mabuchi, E. J. Morris, P. S. Tanwar, L. Dobens *et al.*, 2008 The *Drosophila* homolog of human tumor suppressor TSC-22 promotes cellular growth, proliferation, and survival. Proc. Natl. Acad. Sci. USA 105: 5414–5419.

Yucel, J. K., J. D. Marszalek, J. R. McIntosh, L. S. Goldstein, D. W. Cleveland *et al.*, 2000 CENP-meta, an essential kinetochore kinesin required for the maintenance of metaphase chromosome alignment in Drosophila. J. Cell Biol. 150: 1–11.

Communicating editor: R. Anholt

GENETICS

Supporting Information
http://www.genetics.org/content/suppl/2011/09/16/genetics.111.132993.DC1

Identification and Characterization of Genes Required for Compensatory Growth in *Drosophila*

Abigail R. Gerhold, Daniel J. Richter, Albert S. Yu, and Iswar K. Hariharan

DOI: 10.1534/genetics.111.132993

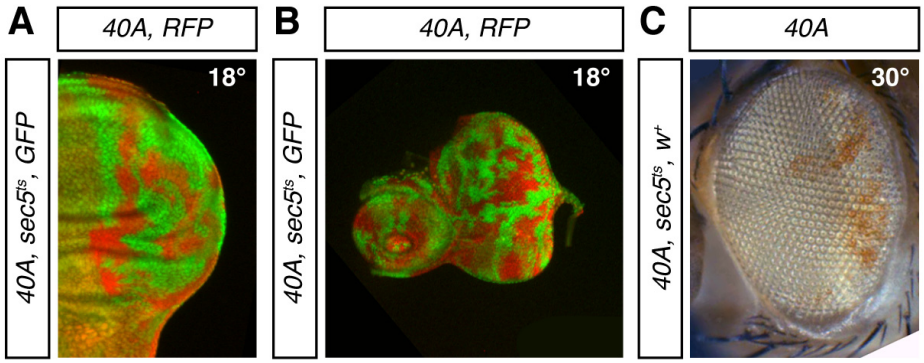

Figure S1 Very little heterozygous tissue remained in mosaic discs generated with either *en-GAL4, UAS-FLP* (A) or *ey-FLP* (B-C). (A-B) A posterior compartment of a mosaic wing disc generated with *en-GAL4, UAS-FLP* (A) and an eye-antennal mosaic disc generated with *ey-FLP* (B). $sec5^{ts}$ clones are GFP-positive (green). Sister clones are RFP-positive (red). Heterozygous cells are yellow and were largely absent. Larvae were maintained at 18° to prevent ablation of homozygous $sec5^{ts}$ tissue and were dissected at the wandering stage (C) An adult eye following $sec5^{ts}$-ablation. Wild-type tissue lacks pigmentation (white) and comprised the majority of the adult eye. Residual heterozygous cells or non-ablated $sec5^{ts}$ cells are pigmented (orange) and remained only in the posterior portion of the adult eye.

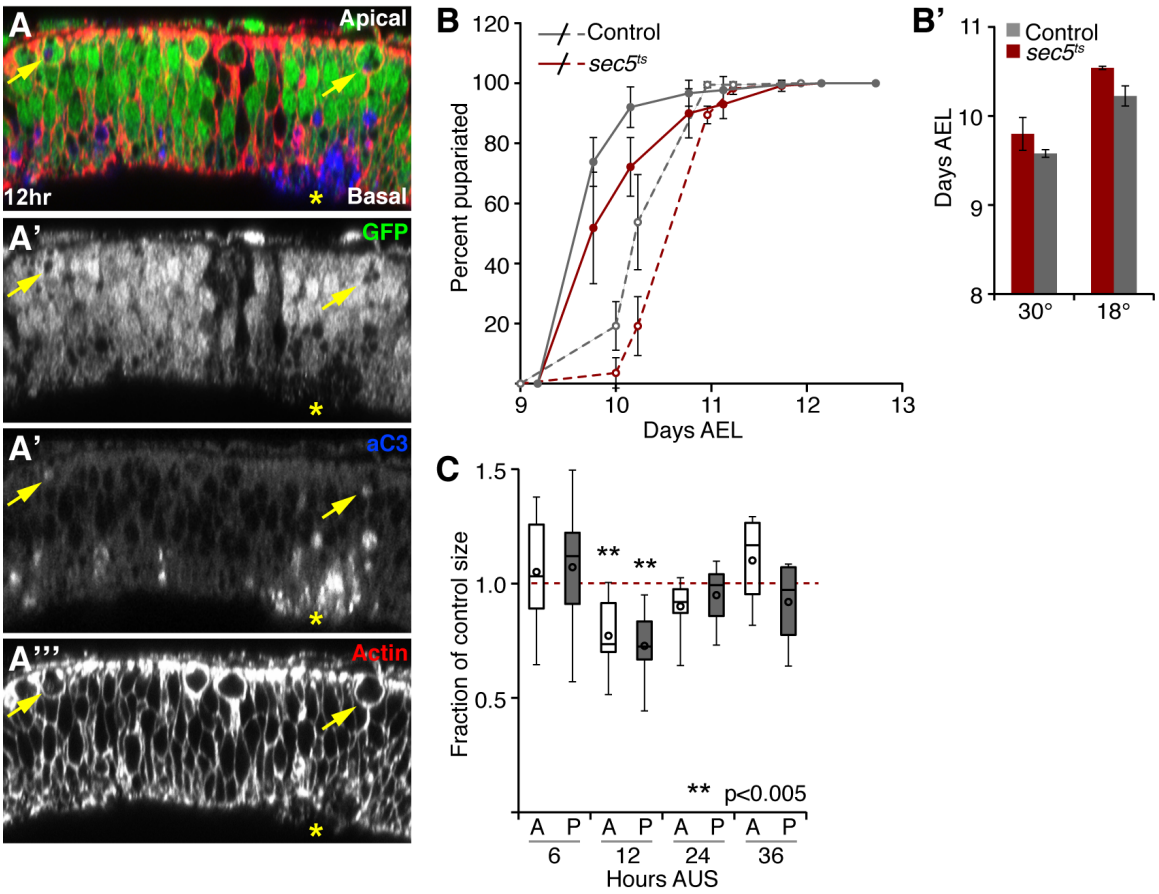

Figure S2 (A) Dying *sec5*^{ts} cells were cleared by a combination of basal extrusion and engulfment. Discs were dissected 12 hours AUS. Anti-cleaved Caspase3 (aC3, blue) marks dying cells, *sec5*^{ts} cells are GFP-negative (green), Phalloidin (Actin, red) outlines cells. Arrows show engulfed GFP-negative, cleaved Caspase3-positive apoptotic bodies within GFP-positive neighboring cells. Asterisk shows basally extruded GFP-negative apoptotic bodies. A single z-slice is shown. Apical is up; basal is down. (B-B') *sec5*^{ts} ablation did not delay the larval to pupal transition. (B) Developmental timing of pupariation for *sec5*^{ts} and control animals. Shifted 30°C ablated experiments shown as solid lines; 18°C non-ablated experiments shown as dashed lines (B') Calculated average time (dAEL) to 50% pupariation from data in (B). *sec5*^{ts} 30°C 9.8 +/- 0.2, control 30°C 9.6 +/- 0.04, *sec5*^{ts} 18°C 10.5 +/- 0.02, control 18°C 10.2 +/- 0.1. (C) The anterior compartment of ablated discs was also reduced in size at 12 hours AUS. The posterior compartment data (Figure 1, H) was shown for comparison.

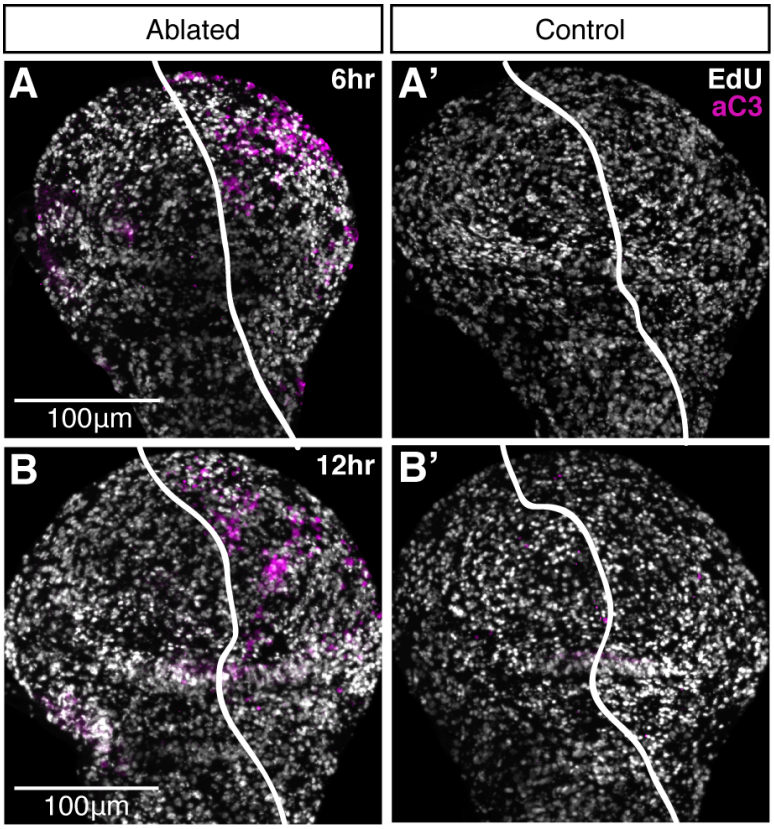

Figure S3 Localized proliferation was not observed by EdU incorporation in proliferating cells. EdU (white) labels proliferating cells, anti-cleaved Caspase3 (aC3, magenta) marks dying cells. White lines mark the approximate A-P boundary as assessed by GFP. Posterior is to the right. Scale bar is 100µm. (A-A') Discs dissected from ablated (A) and control (A') animals 6 hr AUS. (B-B') Discs dissected from ablated (B) and control (B') animals 12 hr AUS.

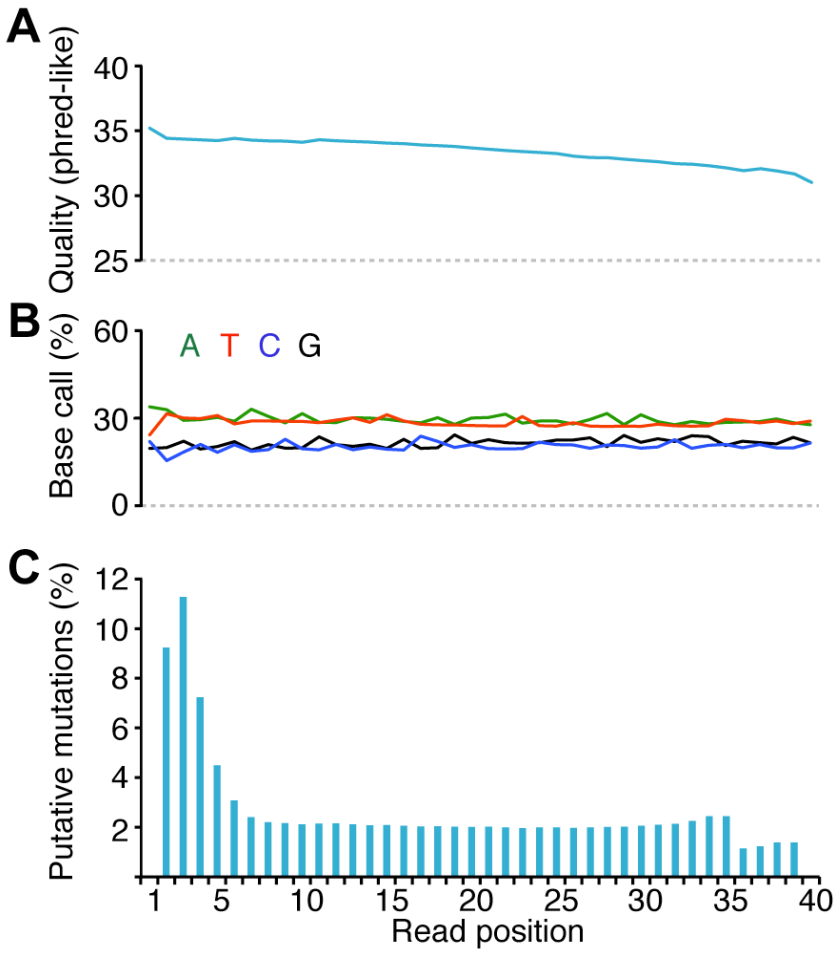

Figure S4 A bias in sequencing quality scores or base composition did not explain the disproportionate number of mutations found at early read positions. (A) The average sequencing quality as a function of read position is shown. Data shown represents the average of the mean quality scores from all sequencing runs. (B) The base composition at each read position was calculated by averaging the mean % A, T, C and G at each position from each sequencing run. No base bias was evident across the read length. (C) The percentage of predicted mutations at each sequencing read position (Figure 6, E) is shown for comparison.

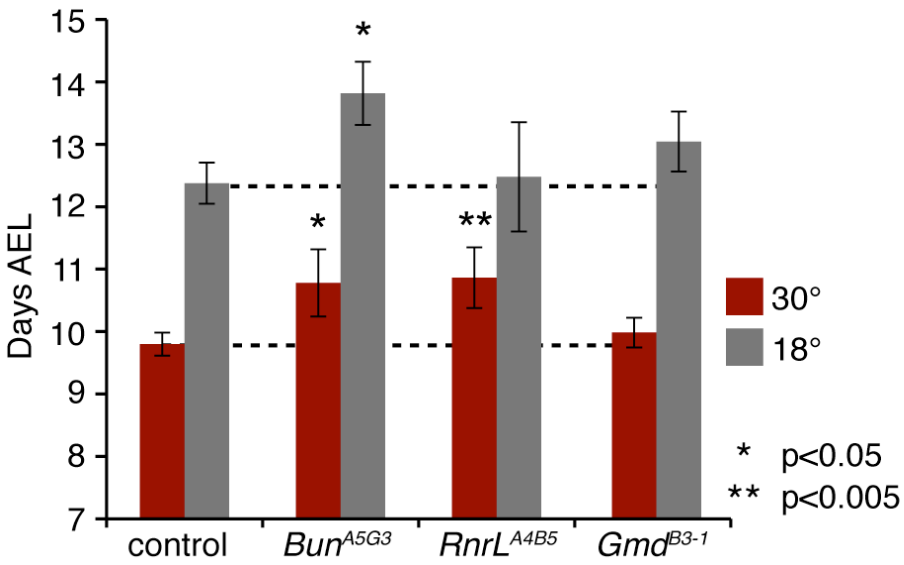

Figure S5 Developmental timing of pupariation of ablated (30°C) or non-ablated (18°C) *Bun*^{A5G3}, *RnrL*^{A4B5} and *Gmd*$^{B3-1}$ animals as compared to control. All animals were crossed to the *sec5*^{ts} wing disc ablation system. One set of animals were shifted to 30°C at 7.5 dAEL, shown in red. A second set was maintained at 18°C, shown in dark grey. The calculated average time (dAEL) to 50% pupariation is shown. Error bars show one STDEV. Dashed lines mark the average time to 50% pupariation for the parental control. Developmental timing was relatively unaffected at 18°C in *Gmd*$^{B3-1}$ and *RnrL*^{A4B5} animals, suggesting that the adult phenotype was not due to accelerated development. Ablated *RnrL*^{A4B5} animals showed a slight delay in pupariation, suggesting that the inability of these animals to compensate might result in a developmental delay. Animals carrying the *bun*^{A5G3} were delayed under both conditions, indicating that these animals were at a slightly earlier development stage at the time of temperature shift. The delayed development of these animals could account for the reduced size of the wing discs (Figure 7, E), as these animals would be "younger" at the time of dissection; however, the resulting adult wings were also reduced in size when compared both to control ablated wings (Figure 7, A) and to *bun*^{A5G3} non-ablated 18°C control wings (data not shown), suggesting that loss of *bun* prevents full recovery of the disc after *sec5*^{ts} ablation.

File S1

Supporting Materials and Methods

Drosophila Stocks

w; P{mw+, ubi-GFP.nls}, sec5^{ts}, FRT40A, en-GAL4, UAS-FLP/CyO

y, w, ey-FLP; P{mw+, ubi-GFP.nls}, sec5^{ts}, FRT40A/SM6-TM6b

w; P{mw+, ubi-RFP.nls}, FRT40A

w; FRT40A

Immunohistochemistry

Antibodies used for supplemental data were rabbit anti-cleaved Caspase3 (1:100, Cell Signaling); mouse anti-GFP (1:500, Roche). Phalloidin was used to stain the actin cytoskeleton and outline cells (1:200, Sigma). Click-iT EdU labeling kit (Invitrogen) was used to mark cells in S-phase. Incorporation and detection was performed according to manufacturer's instructions. A 10 minute incubation in 10μM EdU was used. Images of eye and wing imaginal discs shown in Supplemental Figure 1 were captured on a Zeiss Axio Imager M1 and processed using Adobe Photoshop.

Developmental timing

Eggs were collected on agar grape juice plates at room temperature for 4-6 hours. After 48 hours at 18°C, 55 L1 larvae per a vial were transferred to standard fly food supplemented with fresh yeast paste. Vials were either maintained at 18°C or shifted to 30°C 7.5 dAEL for 48 hours, after which they were returned to 18°C. Pupae were counted every 10-14 hours until all animals had pupariated. Data are presented as the fraction of larvae pupariated or the time to 50% pupariated. Data points represent the average of at least 4 vials. Error bars are one STDEV.